haematologica
Journal of the Ferrata Storti Foundation

Mutual regulation of CD4+ T cells and intravascular fibrin in infections

by Tonina T. Mueller, Mona Pilartz, Manovriti Thakur, Torben LangHeinrich, Junfu Luo, Rebecca Block, Jonathan K. L. Hoeflinger, Sarah Meister, Flavio Karaj, Laura Garcia Perez, Rupert Öllinger, Thomas Engleitner, Jakob Thoss, Michael Voelkl, Claudia Tersteeg, Uwe Koedel, Alexander Zigman Kohlmaier, Daniel Teupser, Malgorzata Wygrecka, Haifeng Ye, Klaus T. Preissner, Helena Radbruch, Sefer Elezkurtaj, Matthias Mack, Philipp von Hundelshausen, Christian Weber, Steffen Massberg, Christian Schulz, Roland Rad, Samuel Huber, Hellen Ishikawa-Ankerhold, and Bernd Engelmann

Received: November 5, 2023.
Accepted: March 25, 2024.

Citation: Tonina T. Mueller, Mona Pilartz, Manovriti Thakur, Torben LangHeinrich, Junfu Luo, Rebecca Block, Jonathan K. L. Hoeflinger, Sarah Meister, Flavio Karaj, Laura Garcia Perez, Rupert Öllinger, Thomas Engleitner, Jakob Thoss, Michael Voelkl, Claudia Tersteeg, Uwe Koedel, Alexander Zigman Kohlmaier, Daniel Teupser, Malgorzata Wygrecka, Haifeng Ye, Klaus T. Preissner, Helena Radbruch, Sefer Elezkurtaj, Matthias Mack, Philipp von Hundelshausen, Christian Weber, Steffen Massberg, Christian Schulz, Roland Rad, Samuel Huber, Hellen Ishikawa-Ankerhold, and Bernd Engelmann.
Mutual regulation of CD4+ T cells and intravascular fibrin in infections.
Haematologica. 2024 Apr 4. doi: 10.3324/haematol.2023.284619 [Epub ahead of print]

Mutual regulation of CD4$^+$ T cells and intravascular fibrin in infections

Tonina T. Mueller[1,2+#], Mona Pilartz[1+], Manovriti Thakur[1+], Torben LangHeinrich[1], Junfu Luo[1], Rebecca Block[1], Jonathan K.L. Hoeflinger[1], Sarah Meister[1], Flavio Karaj[1], Laura Garcia Perez[3], Rupert Öllinger[4], Thomas Engleitner[4], Jakob Thoss[1], Michael Voelkl[1], Claudia Tersteeg[5], Uwe Koedel[6], Alexander Zigman Kohlmaier[1], Daniel Teupser[1], Malgorzata Wygrecka[7], Haifeng Ye[8], Klaus T. Preissner[9], Helena Radbruch[10], Sefer Elezkurtaj[11], Matthias Mack[12], Philipp von Hundelshausen[13], Christian Weber[13], Steffen Massberg[2], Christian Schulz[2], Roland Rad[4], Samuel Huber[3], Hellen Ishikawa-Ankerhold[2*], Bernd Engelmann[1*#]

[1]Institut für Laboratoriumsmedizin, Klinikum der Universität München, Ludwig-Maximilians-Universität (LMU), Munich, Germany; [2]Medizinische Klinik I, Klinikum der Universität München, LMU, Munich, Germany; [3]1. Medizinische Klinik und Poliklinik, Universitätsklinikum Hamburg-Eppendorf, Hamburg, Germany; [4]Institut für Molekulare Onkologie und Funktionelle Genomik, Technische Universität München, Munich, Germany; [5]Laboratory for Thrombosis Research, KU Leuven Campus Kulak Kortrijk, Belgium; [6]Neurologische Klinik, Klinikum der Universität München,LMU, Munich, Germany; [7]Center for Infection and Genomics of the Lung (CIGL), Justus-Liebig-Universität, Giessen, Germany; [8]Institute of Regenerative Biology and Medicine, Helmholtz-Zentrum München, Munich, Germany; [9]Institute of Biochemistry, Justus-Liebig-Universität, Giessen, Germany; [10]Institut für Neuropathologie, Charité - Universitätsmedizin, Berlin, Germany; [11]Institut für Pathologie, Charité - Universitätsmedizin, Berlin, Germany; [12]Medizinische Klinik II, University of Regensburg, Regensburg, Germany; [13]Institut für Prophylaxe und Epidemiologie der Kreislaufkrankheiten, Ludwig-Maximilians-Universität, Munich, Germany

[+]These authors equally contributed to the study.

[*]These authors equally contributed to the study.

Short title: Bidirectional T cell-fibrin signaling

Corresponding authors:

Bernd Engelmann, Institut für Laboratoriumsmedizin, Klinikum der Universität München, Ludwig-Maximilians-Universität, Marchioninistr. 15, 81377 München, Germany. Bernd.Engelmann@med.uni-muenchen.de. Tel. +49-89-440073243

Tonina T Mueller, Medizinische Klinik I, Klinikum der Universität München, Ludwig-Maximilians-Universität, Marchioninistr. 15, 81377 München, Germany. Tonina.Mueller@med.uni-muenchen.de. Tel. +49-89-440074732

Author contributions

T.T.M., M.P., M.T, T.L., J.K.L.H., S.Me., R.B., F.K., L.G.P., R.O□., T.E., J.L., M.V., H.Y., H.I.- A. performed experiments and evaluated data. T.T.M, H.I.-A., B.E. analyzed data. C.W., A.Z.K., K.T.P., S.H., S.M. contributed to interpretation and presentation of data. C.S., H.I.-A., B.E. coordinated and supervised the study. C.T., M.Wy., H.R., S.E., P.v.H., C.S., D.T., R.R., S.H., M.M., S.M., D.T., U.K. provided resources. B.E., S.M. secured funding. B.E. conceived the study and wrote the manuscript with the help of all other authors.

Competing interests

The authors declare no competing interests.

Acknowledgement

We are grateful to Susanne Pfeiler, Pia Vornewald, Dominic van den Heuvel, Daniel Setzensack, Meike Miller, Anna Titova, Arwa Obaid, Wolfgang Wilfert, Lusine Saroyan and Anastasios Giannou for their contributions at different stages of the study. We would like to kindly thank the Core Facility Bioimaging of the Biomedical Center of LMU Munich, especially Steffen Dietzel, for advice and help. We are grateful to Paul Declerck, Michael Ploug and Thomas Bugge for their helpful advice as well as for providing antibodies. We thank the German Center for Lung Research (DZL) for providing tissue sections from autopsies.

Funding

The study was supported by grants of the Deutsche Forschungsgemeinschaft SFB1321 (to B.E. and S.M), SFB1123 (to S.M. and B.E.) and SFB 914 (to H.I.A., S.M. and C.S.).

Materials & Correspondence

Please direct all requests for materials and correspondence to: Bernd Engelmann, Institut fu□r Laboratoriumsmedizin, Ludwig-Maximilians-Universita□t, LMU Klinikum, Marchioninistr. 15, 81377 Mu□nchen, Germany, Bernd.Engelmann@med.uni-muenchen.de. Tel. +49-89-440073243

Tonina T Mueller, Medizinische Klinik I, Klinikum der Universität München, Ludwig-Maximilians-Universität, Marchioninistr. 15, 81377 München, Germany. Tonina.Mueller@med.uni-muenchen.de. Tel. +49-89-440074732

Abstract

Innate myeloid cells especially neutrophils and their extracellular traps are known to promote intravascular coagulation and thrombosis formation in infections and various other conditions. Innate myeloid cell dependent fibrin formation can support systemic immunity while its dysregulation enhances the severity of infectious diseases. Less is known about the immune mechanisms preventing dysregulation of fibrin homeostasis in infection. During experimental systemic infections local fibrin deposits in the liver microcirculation cause rapid arrest of $CD4^+$ T cells. Arrested T helper cells mostly represent Th17 cells that partially originate from the small intestine. Intravascular fibrin deposits activate mouse and human $CD4^+$ T cells which can be mediated by direct fibrin - $CD4^+$ T cell interactions. Activated $CD4^+$ T cells suppress fibrin deposition and microvascular thrombosis by directly counteracting coagulation activation by neutrophils and classical monocytes. T cell activation, which is initially triggered by IL-12p40- and MHC-II dependent mechanisms, enhances intravascular fibrinolysis via LFA-1. Moreover, $CD4^+$ T cells disfavor the association of the fibrinolysis inhibitor TAFI with fibrin whereby fibrin deposition is increased by TAFI in the absence but not presence of T cells. In human infections thrombosis development is inversely related to microvascular levels of $CD4^+$ T cells. Thus, fibrin promotes LFA-1 dependent T helper cell activation in infections which drives a negative feedback cycle that rapidly restricts intravascular fibrin and thrombosis development.

Introduction

Inflammation and thrombosis are closely coupled responses to infections[1]. Innate immune cells such as neutrophils and monocytes are quintessential activators of fibrin formation and mediators of thrombosis during systemic immune processes. Through expulsion of neutrophil extracellular traps (NETs) neutrophils promote thrombosis via different mechanisms that help to initiate and stabilize developing thrombi[2]. Monocytes trigger fibrin formation by activating the NLRP3 inflammasome and subsequent release of tissue factor (TF) through pyroptosis[3].

During systemic infections activation of intravascular coagulation promotes the formation of microvascular thrombi that can restrict the dissemination and survival of bacteria[4]. Innate immune cell-controlled coagulation activation inside the microvasculature can thus participate in antimicrobial defense, analogous to the protective function of coagulum formation in evolutionarily ancient organisms[5]. So far, it is only incompletely known whether immune cells apart from innate leukocytes, especially cells of the lymphocyte lineage, participate in controlling intravascular coagulation and microvascular thrombosis during infections. Aberrant fibrin generation and dysregulated micro- and macrovascular thrombosis can be detrimental consequences of innate immune responses to severe infections. Pathological thrombosis in connection with inflammation critically aggravates the morbidity and mortality of SARS-CoV-2 infections[6] and sepsis[7]. Hence it is of particular interest to dissect the endogenous mechanisms that restrict intravascular fibrin generation in infection. Endothelial cells are known to be critical protectors against excessive fibrin deposition in the microcirculation such as via production of anticoagulant molecules including activated protein C and local stimulation of fibrinolysis.

Here we identify close bidirectional connections between $CD4^+$ T cells and microvascular fibrin homeostasis in vascular infection. Local fibrin deposits are shown to promote the arrest and LFA-1 dependent activation of $CD4^+$ T cells in the microcirculation. Activated T helper cells rapidly restrict innate myeloid-cell driven thrombosis at and, favored by T cell migration, distant from their arrest sites by stimulating fibrinolysis and disabling fibrinolysis inhibition

Methods

Mice

Male and female mice (10-14 weeks old, age-matched) were infected with *E. coli* (3.2×10^8) or *S. pneumoniae* (1×10^8) via tail vein injection. Rivaroxaban (Santa Cruz) was injected at 3 mg/kg body weight 4h before infection. Cell depletion and neutralization was performed as

described in the supplementary methods. All animal experiments were approved by the local authorities (Regierung von Oberbayern).

Kaede experiments

The small intestine of *kaede* x *Il17a*^{Katushka} mice was surgically exposed to photoconvert the accessible cells (dorsal and ventral) with BlueWave LED Prime UVA (Dymax) for 2x 30s. 24h later mice were infected with *E. coli*[8]. Flow cytometry was performed as described in supplementary methods.

Isolation and Migration of CD4$^+$ T cells

For intravital imaging or adoptive transfer experiments mouse CD4$^+$ T cells were isolated from spleen of uninfected C57BL/6J donor mice. Blood was collected from healthy human donors as approved by the local ethics committee of the Medical Faculty of LMU Munich. Human CD4$^+$ T cells were isolated from peripheral blood according to the manufacturer´s instructions (CD4$^+$ T Cell Isolation Kit, 130-096-533, Miltenyi Biotec). Cells were incubated on Fibrin or poly-L-ornithine coated microscopic glass slides with α-human CD3 antibody (5 µg/ml, HIT3a, Biolegend) with α-human CD28 antibody (5 µg/ml, CD28.2, Biolegend) or treated with either an IgG control or an anti-human LFA-1 antibody (20 µg/ml, BioXCell). Isolated CD4$^+$ T cells were fixed, blocked and incubated with AF647-labeled αCD69 antibody (1 µg/ml, Biolegend) and Dapi (1 µg/ml, Sigma Aldrich). For each experiment at least 10 visual fields (225 x 225 µm) per donor were analysed by confocal microscopy.

Immunohistochemistry

The murine livers and lungs were collected and fixed with neutral buffered 4% PFA at 4˚C for 1h, dehydrated in 30% sucrose for 24h at 4˚C and embedded in Tissue Tek. 10 µm cryosections were fixed in 4% PFA, washed and blocked with 2% BSA solution or with 10% goat serum (Sigma Aldrich). For permeabilization, 0.1%-0.3% Triton-X 100 was added. Tissue sections were incubated with unlabeled or labeled primary antibodies for 1h at room temperature or overnight at 4°C. The labeling of primary antibodies was performed according to the manufacturer´s instructions (A20181, Thermo Fisher Scientific).

Tissue samples from the lung of patients with acute respiratory distress syndrome caused by infections with SARS-CoV-2 (n=12) or influenza virus (n=8) were obtained from autopsies. SARS-CoV-2 or influenza infections were diagnosed by PCR ante mortem. Mean age was 78.7±2.6 (SARS-CoV-2) and 68.1±5.5 years (Influenza). 41.7% (SARS-CoV-2) and 37.5% (Influenza) of the patients were female, respectively (FigS6A).

Plasmin formation by mouse and human T helper cells

To analyze the fibrinolytic activity of different immune cells, plasmin formation was determined. For clot preparation, plasminogen (1 mg/ml, Sigma Aldrich) and fibrinogen (2.5 mg/ml, Sigma Aldrich) (1:80 vol/vol) were mixed and thrombin was added (4U/ml; 3:1 vol/vol, Sigma Aldrich). The suspension was incubated for 1h at 37°C in 96 well plates. Afterwards chromogenic substrate S-2251 (1.5 mmol/l, Diapharma) and T helper cells (mouse: 100,000 cells/well, human: 100,000 cells/well) were added. In the case of human T helper cells, T cells were activated on fibrin-coated 96 well plates in the presence of αCD3 and αCD28 antibodies as described above, and plasmin formation registered in situ. The optical density (A_{405}) was determined every 5 to 10min to measure the protease activity of the generated plasmin.

RNAseq

$CD4^+$ T cells were isolated from the liver of uninfected and infected WT mice as described above. Library preparation for bulk-sequencing of poly(A)-RNA was done largely as described previously [9].

Results

$CD4^+$ T cells restrict intravascular fibrin deposition in early systemic infections

To identify the immune cells regulating intravascular coagulation during systemic infections with E. coli we imaged nucleated cells arrested in the liver microcirculation, the major site of bacterial colonization. Neutrophils ($Ly6G^+$), classical ($Ly6C^+Ly6G^-$) and non-classical monocytes ($CX3CR1^+Ly6C^-$), $CD4^+$ T cells and B cells ($CD19^+$) were recruited to the liver microcirculation with different kinetics (Fig. 1a). T helper cells represented largely Th17 cells ($ROR\gamma T^+$) and regulatory T cells ($Foxp3^+$; T_{regs}) and lower amounts of Th2 cells, while B cells were mostly B1a cells ($CD5^+$) (Fig. 1A; Supplementary Fig. 1A).

Since the role of T helper cells in systemic infections and coagulation is incompletely defined and T helper cells were recruited as abundantly as myeloid cells we analyzed their transcriptomic profiles. Unbiased analyses of the mRNA expressions of liver-resident $CD4^+$ T cells indicated the enrichment of genes predicted to be involved in innate immune responses (Fig. 1B; confirming proinflammatory functions of T helper cells[10]). Remarkably, the gene cluster with the second highest enrichment score represented T cell genes implicated in blood coagulation. Among the coagulation genes regulators of fibrinolysis predominated during early infection (Fig. 2A).

Microvascular fibrin deposition was highest 3 h after infection (Supplementary Fig. 1B). Analyses of fibrin formation in systemic blood at the same time

point indicated no change in coagulation time or other parameters compared to non-infected controls (Supplementary Fig. 1C). tPA levels in systemic blood were increased by infection consistent with increased fibrinolysis (Supplementary Fig. 1D). Imaging of coagulation proteins in the microcirculation showed that basic mediators of fibrinolysis (plasminogen, tPA, uPA, uPAR) were associated with $CD4^+$ T cells at the peak of fibrin formation (Fig. 2B). Tissue factor (TF), the initiator protein of coagulation, was mostly associated with classical monocytes and neutrophils (Fig. 2B[11–13]). Overall, $CD4^+$ T cells represented the immune cell with the highest association of fibrinolysis activators (Fig. 2B). Comparisons between different T helper cell subtypes indicated that most of the Th17 cells and part of the regulatory T cells (T_{regs}) and Th2 cells were positive for the plasminogen activator uPA (Supplementary Fig. 1E). Next, we investigated whether T helper cells regulated fibrin deposition. Depletion of T helper cells strongly reduced circulating $CD4^+$ T cells (Supplementary Fig. 1F). Moreover, arrest of $CD4^+$ T cells in the liver microcirculation was completely abolished by depletion of $CD4^+$ T cells (from 5.2 to 0.07 $CD4^+$ T cells/visual field). $CD4^+$ T cell depletion sharply increased fibrin deposition in microvessels of the liver and the lung (Fig. 3A,B). Particularly, the absence of $CD4^+$ T cell enhanced microvascular thrombosis (Fig. 3A). Also, fibrin deposition and thrombus formation occasionally observed in larger vessels were increased after $CD4^+$ T cell depletion (Fig. 3C). AST and ALT levels, indicators of liver tissue damage, were largely unchanged in early infection both in the presence and absence of T cells (Supplementary Fig. 1G). Thus $CD4^+$ T cells inhibited fibrin deposition and development of thrombosis during systemic infection.

In contrast to the changes by T helper loss, depletion of neutrophils (which reduced circulating neutrophils by 93%) decreased fibrin deposition (Supplementary Fig. 2A). Moreover, intravascular fibrin was reduced in the absence of classical monocytes (Supplementary Fig. 2A). Thus $CD4^+$ T cells rapidly suppress fibrin deposition during initial fibrin formation and thereby counteract procoagulant neutrophils and classical monocyte. In advanced stages of venous thrombosis and under non-infectious conditions, neutrophils and $CD4^+$ T cells especially regulatory T cells (T_{regs})[14] cooperatively enhance resolution of venous thrombosis[15]. Depletion of T_{regs} only slightly increased fibrin deposition in early systemic infection (Supplementary Fig. 2B). This suggested that other T cell subtypes such as Th17 cells contributed predominantly to restrict fibrin deposition and indicated that under infectious conditions $CD4^+$ T cells acted as direct antagonists of innate myeloid cells. Similar to *E.coli* infection, infection with the Gram-positive *S.pneumoniae* triggered microvascular fibrin generation in the liver and the lung (Fig.

3D). $CD4^+$ T cell depletion also amplified fibrin deposition in streptococcal infection (Fig. 3D).

$CD4^+$ T cells stimulate fibrinolysis in early infection

To dissect the activity of T cell-associated fibrinolysis activators $CD4^+$ T cells were isolated from uninfected and infected mice and analyzed for their ability to support formation of plasmin ex vivo. T cells from infected mice and, less so, from uninfected mice, promoted plasmin formation (Fig. 4A). Moreover, isolated human T helper cells supported plasmin formation which was enhanced by TCR-dependent T cell activation (Supplementary Fig. 2C[16]). Next, activated mouse $CD4^+$ T cells were adoptively transferred into factor VIIa-supplemented mice (to enhance fibrin levels). Activated T cells decreased fibrin deposition which was prevented by pretreatment of the cells with fibrinolysis inhibitor EACA (Supplementary Fig. 2D). Furthermore, neutralization of uPA in vivo, which was preferentially associated with T cells (Fig. 2B), enhanced fibrin deposition in control mice, but not in T helper cell-depleted mice (Fig. 4B).

Since $CD4^+$ T cells promoted fibrinolysis during the initial increase in fibrin deposition, we studied the involvement of thrombin activatable fibrinolysis inhibitor (TAFI) which connects coagulation to fibrinolysis[17,18]. Neutralization of TAFI activity by anti-TAFI antibody that specifically targets activated TAFI did not affect fibrin deposition in control mice consistent with earlier work[19]. Yet, anti-TAFI antibody suppressed fibrin formation in $CD4^+$ T cell-depleted mice (Fig. 4C). Inhibition of TAFI by CPI (also preferentially inhibiting activated TAFI) confirmed that activated TAFI regulated fibrin deposition in the absence but not in presence of T helper cells (Fig. 4D).

Imaging of the TAFI localization in the microcirculation of control mice indicated a higher association of TAFI with $CD4^+$ T cells compared to other types of leukocytes (Fig. 4E). Apart from its cellular association, TAFI was mainly associated with fibrin deposits[20] (Fig. 3F,G). Together, this is consistent with regulation of fibrinolysis on both cellular and fibrin surfaces[21]. After $CD4^+$ T cell depletion, TAFI colocalized almost exclusively with the increased fibrin-covered areas (Fig. 4F,G). The extent of TAFI association with fibrin was enhanced in $CD4^+$ T cell depleted mice (Fig. 4F). Thus, $CD4^+$ T cells prevented fibrinolysis inhibition by TAFI which could be mediated in part by their ability to reduce the association of TAFI with fibrin.

Intravascular fibrin promotes T cell arrest and activation

Since $CD4^+$ T cells partially colocalized with fibrin and components of the coagulation

system affect T cell recruitment[22], we next investigated whether fibrin contributed to T cell arrest. In mice deficient for coagulation factor XII (*f12*$^{-/-}$), in which fibrin deposition was inhibited compared to control mice (Supplementary Fig. 3A), arrest of CD4^{+} T cells was strongly reduced compared to WT mice (Fig. 5A). In mice treated with rivaroxaban, an inhibitor of coagulation factor Xa that suppressed fibrin formation, arrest of T cells, particularly of Th17 cells, was lowered (Supplementary Fig. 3B,C). Conversely, in plasminogen-deficient mice (*plg*$^{-/-}$) with increased fibrin deposition (from 8.2 ± 0.3 (WT) to 22.8 ± 3.0% fibrin-covered area (*plg*$^{-/-}$); n = 3 mice/group, $p < 0.05$), immobilization of CD4^{+} T cells and especially of Th17 cells were augmented (Fig. 5B).

T cells recovered at the peak of fibrin formation highly expressed genes involved in T cell activation (Supplementary Fig. 3D). Notably, CD4^{+} T cells colocalizing with fibrin and expressed the activation markers CD69 and CD38 (Fig. 5C). Besides their presence in microvessels, activated CD4^{+} T cells were detected in association with thrombi in larger vessels (Supplementary Fig. 3E). Rivaroxaban decreased the levels of arrested CD69^{+} T cells substantially (Fig. 5D). Furthermore, T cell activation was decreased in *f12*$^{-/-}$ mice compared to WT mice (Fig. 5E). Rivaroxaban also reduced IFNγ^{+}T cells which are another sign of early T cell activation. (Fig. 5F).

The high percentages of CD69^{+}T cells in early infection could suggest that T cell activation may be mediated at least in part by TCR-independent cytokine (or "bystander") activation[23]. To dissect the contributions TCR-dependent and/or -independent T cell activation, we prevented TCR dependent T cell activation with anti-MHC-II antibody. We also used anti-IL-12p40 antibody to inhibit IL-12- and IL23-mediated T cell activation thus preventing in particular cytokine-mediated activation of Th17 cells[24]. MHC-II inhibition reduced the amount of activated T cells (Fig. 5F). Moreover, anti-IL-12p40 antibody decreased T cell activation (Fig. 5F). Particularly, the levels of activated T cells (CD69^{+} IFNγ^{+}) colocalizing with fibrin were decreased by neutralizing MHC-II or IL-12p40 inhibition (Supplementary Fig. 3F). Thus early CD4^{+} T cell activation by fibrin was supported by TCR- and cytokine-dependent mechanisms.

LFA-1 mediates T helper cell migration and fibrin-dependent T cell activation

We next analyzed the source and intravascular movements of the T cells regulating coagulation. To investigate their intestinal origin[25], we photoconverted cells in the small intestine of Kaede mice by UV light to emit red fluorescence instead of green fluorescence (Supplementary Fig. 4A)[26]. 24h later systemic infection was induced with *E. coli*.

Photoconverted T helper cells were detected in the infected livers and to a lesser extent in the lungs (Supplementary Fig. 4B). Most of the intestine-derived T helper cells in the liver represented Th17 cells.

We used multi-photon intravital microscopy to track the movements of CMTPX-labeled $CD4^+$ T cells inside the liver microvasculature. We observed a rapid arrest of part of the circulating T cells while other T cells crawled unidirectionally along the vessel wall or performed alternating movements with and against the blood flow (Fig. 6A,B; Supplementary Video S1). Real-time imaging of T helper cell movements showed that neutralization of the major T cell integrin LFA-1[27] with anti-LFA-1 decreased the unidirectional T cell crawling along the vessel wall (Fig. 6C). In contrast, suppression of fibrin formation by rivaroxaban did not alter T cell migration (Supplementary Fig.5A, Supplementary Video S2). Moreover, neutralization of LFA-1 did not change T cell arrest (Fig. 6C). In contrast, it decreased T cell activation substantially, especially activated T cells that were fibrin-associated (Fig. 6D; Supplementary Fig. 5B).

Next, we studied the role of fibrin for T cell activation in human $CD4^+$ T cells in vitro. T cells adhering to poly-L-ornithine coated surfaces where activated via the TCR. The increase in CD69 expression thus observed was unaffected by inhibition of LFA-1 (Fig. 6E). Fibrin-coated surfaces noticeably enhanced activation of T cells. T cell activation by fibrin was largely suppressed by LFA-1 inhibition (Fig. 6E). Contrary to the effect of fibrin on T cell activation, fibrin did not affect migration of human T cells (Fig. 6F), agreeing with the in vivo observations (Supplementary Fig. 4C). Inhibition of LFA-1 markedly decreased the fibrinolytic activity of the activated T cells (Supplementary Fig. 5C). Thus, LFA-1 mediated both T cell migration and T cell activation-dependent fibrinolysis which allowed $CD4^+$ T cells most likely to inhibit fibrin deposition both at and distant from sites of T cell arrest.

Microvascular $CD4^+$ T cells and thrombosis in human infections

Pulmonary thrombosis is a deleterious consequence of aberrant immune activation in severe infections including SARS-CoV-2 infection[28,29]. We analyzed autopsies from patients with SARS-CoV-2 infections and compared them with autopsies from patients with influenza virus infections (Supplementary Fig. 6A). $CD4^+$ T cells were visualized in different vascular beds of the lung to explore their potential role in thrombosis. The number of $CD4^+$ T cells detected in microvessels and larger vessels in patients with SARS-CoV-2 infections was lower compared to patients infected with influenza virus (Fig. 7A,B). Thrombotic vessel occlusions were massively increased and pulmonary thrombi tended to be elevated in SARS-

CoV-2 infections compared to influenza virus infection (Fig. 7C, Supplementary Fig. 6B). TAFI strongly colocalized with fibrin-rich thrombi in SARS-CoV-2 infections (Fig. 7D) but barely with intraluminal immune cells. Thus, the enhanced fibrin depositions and TAFI localizations in human infections with strongly reduced microvascular T cell levels resembled the changes in T cell-depleted mice. Overall, thrombosis formation in lung vessels during viral infections exhibited an inverse association with microvascular $CD4^+$ T cell levels (Fig. 7E).

Discussion

Innate immune cells including monocytes and neutrophils critically promote intravascular fibrin formation and thereby favor the development of different types of micro- and macrovascular thrombosis[1–5]. They initiate coagulation via the TF-initiated extrinsic pathway of coagulation and propagate fibrin generation by formation of NETs. Due to the potentially deleterious consequences of thrombotic vessel occlusions intravascular coagulation needs to be maintained in a homeostatic balance thus disfavoring pathological thrombosis. Although endothelial cells can efficiently protect against excessive intravascular fibrin generation, their anticoagulant and profibrinolytic functions are often compromised during infections, especially at sites of thrombus formation, or they may even be converted into procoagulant mediators[30]. This suggests that additional mechanisms are required to prevent excessive intravascular fibrin and development of thrombosis in infections.

Our study shows that mutual interactions between $CD4^+$ T cells and fibrin establish an efficient negative feedback cycle suppressing intravascular fibrin and microvascular thrombosis during infections. Since T helper cells curtail fibrin deposition during the initial rise in fibrin formation they act as direct antagonists of procoagulant innate myeloid cells, especially counteracting neutrophil dependent fibrin formation. It is well possible that increases in proinflammatory cytokines such as IL-1β, TNFα or IL-6 as induced by systemic infection contribute to regulate the inhibitory and enhancing effects of T helper cells and innate myeloid cells, respectively, on intravascular fibrin deposition.

Intravital imaging and immunohistochemistry analyses reveal that fibrin deposits drive the arrest and LFA-1 dependent activation of $CD4^+$ T cells. The arrested T cells mostly represent Th17 cells that are recruited at least in part from the intestine, a major site of residence of Th17 cells. T helper cell activation appears to require direct fibrin-LFA-1 interactions and is in part mediated by IL-12p40, a component of both

IL-12 and IL-23[31] that preferentially targets Th17 cells[24], as well as by MHC-II dependent mechanisms. Activation and migration of $CD4^+$ T cells in turn suppresses fibrin deposition throughout the vasculature by neutralization of TAFI-induced fibrinolysis inhibition and direct stimulation of fibrinolysis. During early infection, $CD4^+$ T cells are indeed the major intraluminal carriers of fibrinolysis regulators including plasminogen and their activators. T helper cell dependent inhibition of TAFI is shown to be related to the ability of the T cells to prevent the association of TAFI with fibrin, a prerequisite for TAFI-dependent cleavage of C-terminal lysine residues in fibrin[32] and subsequent fibrinolysis inhibition. This mechanism could contribute to explain why (at presumably normal T cell levels) TAFI deficiency does not result in substantial changes in fibrin formation and thrombosis development[19].

Dysregulations of coagulation are characteristics of severe SARS-CoV-2 infections and might sustain in part long-term sequelae of Covid-19 infections[33–35]. Since activated $CD4^+$ T cells promote fibrinolysis and their loss increases intravascular fibrin via TAFI, the inverse relations between T cell arrest and thrombosis observed here suggest that also in human infections $CD4^+$ T cells might protect from pathological thrombosis. Consequently, lymphopenic conditions, a common feature of fatal infections and other diseases[36–38], critically dysregulate thrombosis per se. The opposing effects of neutrophils vs. $CD4^+$ T cells, the major circulating lymphocyte fraction in human blood, suggest why increased neutrophil/lymphocyte ratios (for example[39]) predispose for different types of pathological thrombosis.

References

1. Iba T, Levy JH. Inflammation and thrombosis: roles of neutrophils, platelets and endothelial cells and their interactions in thrombus formation during sepsis. J Thromb Haemost. 2018;16(2):231-241.
2. Van Bruggen S, Martinod K. The coming of age of neutrophil extracellular traps in thrombosis: Where are we now and where are we headed? Immunol Rev. 2023;314(1):376-398.
3. Wu C, Lu W, Zhang Y, et al. Inflammasome Activation Triggers Blood Clotting and Host Death through Pyroptosis. Immunity. 2019;50(6):1401-1411.
4. Engelmann B, Massberg S. Thrombosis as an intravascular effector of innate immunity. Nat Rev Immunol. 2013;13(1):34-45.
5. Opal SM, Esmon CT. Bench-to-bedside review: Functional relationships between coagulation and the innate immune response and their respective roles in the pathogenesis of sepsis. Crit Care. 2002;7(1):23-38.
6. Bonaventura A, Vecchié A, Dagna L, et al. Endothelial dysfunction and immunothrombosis as key pathogenic mechanisms in COVID-19. Nat Rev Immunol. 2021;21(5):319-329.
7. van der Poll T, van de Veerdonk FL, Scicluna BP, Netea MG. The immunopathology of sepsis and potential therapeutic targets. Nat Rev Immunol. 2017;17(7):407-420.
8. Tomura M, Yoshida N, Tanaka J, et al. Monitoring cellular movement in vivo with photoconvertible fluorescence protein “Kaede” transgenic mice. Proc Natl Acad Sci USA. 2008;105(31):10871-10876.
9. Parekh S, Ziegenhain C, Vieth B, Enard W, Hellmann I. The impact of amplification on differential expression analyses by RNA-seq. Sci Rep. 2016;6:25533.
10. Kedl RM, White JT. Foreign antigen-independent memory-phenotype CD4+ T cells: a new player in innate immunity? Nat Rev Immunol. 2018;18(3):1.
11. Skendros P, Mitsios A, Chrysanthopoulou A, et al. Complement and tissue factor–enriched neutrophil extracellular traps are key drivers in COVID-19 immunothrombosis. J Clin Invest. 2020;130(11):6151-6157.
12. Schechter ME, Andrade BB, He T, et al. Inflammatory monocytes expressing tissue factor drive SIV and HIV coagulopathy. Sci Transl Med. 2017;9(405):eaam5441.
13. Antoniak S, Mackman N. Multiple roles of the coagulation protease cascade during virus infection. Blood. 2014;123(17):2605-2613.
14. Shahneh F, Grill A, Klein M, et al. Specialized regulatory T cells control venous blood clot resolution through SPARC. Blood. 2021;137(11):1517-1526.
15. Nicklas JM, Gordon AE, Henke PK. Resolution of Deep Venous Thrombosis: Proposed Immune Paradigms. Int J Mol Sci. 2020;21(6):2080.

16. Loef EJ, Sheppard HM, Birch NP, Dunbar PR. Plasminogen and plasmin can bind to human T cells and generate truncated CCL21 that increases dendritic cell chemotactic responses. J Biol Chem. 2022;298(7):102112.
17. Sillen M, Declerck PJ. Thrombin Activatable Fibrinolysis Inhibitor (TAFI): An Updated Narrative Review. Int J Mol Sci. 2021;22(7):3670.
18. Nesheim M, Wang W, Boffa M, Nagashima M, Morser J, Bajzar L. Thrombin, Thrombomodulin and TAFI in the Molecular Link Between Coagulation and Fibrinolysis. Thromb Haemost. 1997;78(01):386-391.
19. Nagashima M, Yin Z-F, Zhao L, et al. Thrombin-activatable fibrinolysis inhibitor (TAFI) deficiency is compatible with murine life. J Clin Invest. 2002;109(1):101-110.
20. Satoh T, Satoh K, Yaoita N, et al. Activated TAFI Promotes the Development of Chronic Thromboembolic Pulmonary Hypertension: A Possible Novel Therapeutic Target. Circ Res. 2017;120(8):1246-1262.
21. Chapin JC, Hajjar KA. Fibrinolysis and the control of blood coagulation. Blood Rev. 2015;29(1):17-24.
22. Ryu JK, Petersen MA, Murray SG, et al. Blood coagulation protein fibrinogen promotes autoimmunity and demyelination via chemokine release and antigen presentation. Nat Commun. 2015;6(1):8164.
23. Lee H, Jeong S, Shin E-C. Significance of bystander T cell activation in microbial infection. Nat Immunol. 2022;23(1):13-22.
24. Mills KHG. IL-17 and IL-17-producing cells in protection versus pathology. Nat Rev Immunol. 2023;23(1):38-54.
25. Stockinger B, Omenetti S. The dichotomous nature of T helper 17 cells. Nat Rev Immunol. 2017;17(9):535-544.
26. Krebs CF, Reimers D, Zhao Y, et al. Pathogen-induced tissue-resident memory T_H 17 (T_{RM} 17) cells amplify autoimmune kidney disease. Sci Immunol. 2020;5(50):eaba4163.
27. Walling BL, Kim M. LFA-1 in T Cell Migration and Differentiation. Front Immunol 2018;9952.
28. Ackermann M, Verleden SE, Kuehnel M, et al. Pulmonary Vascular Endothelialitis, Thrombosis, and Angiogenesis in Covid-19. N Engl J Med. 2020;383(2):120-128.
29. Afzali B, Noris M, Lambrecht BN, Kemper C. The state of complement in COVID-19. Nat Rev Immunol. 2022;22(2):77-84.
30. Yau JW, Teoh H, Verma S. Endothelial cell control of thrombosis. BMC Cardiovasc Disord. 2015;15:130.
31. Cooper AM, Khader SA. IL-12p40: an inherently agonistic cytokine. Trends Immunol. 2007;28(1):33-38.

32. Wang W, Boffa MB, Bajzar L, Walker JB, Nesheim ME. A Study of the Mechanism of Inhibition of Fibrinolysis by Activated Thrombin-activable Fibrinolysis Inhibitor. J Biol Chem. 1998;273(42):27176-27181.
33. Morrow AJ, Sykes R, McIntosh A, et al. A multisystem, cardio-renal investigation of post-COVID-19 illness. Nat Med. 2022;28(6):1303-1313.
34. Couzin-Frankel J. Clues to long COVID. Science. 2022;376(6599):1261-1265.
35. Al-Aly Z, Bowe B, Xie Y. Long COVID after breakthrough SARS-CoV-2 infection. Nat Med. 2022;28(7):1461-1467.
36. Moss P. The T cell immune response against SARS-CoV-2. Nat Immunol. 2022;23(2):186-193.
37. Drewry AM, Samra N, Skrupky LP, Fuller BM, Compton SM, Hotchkiss RS. Persistent Lymphopenia After Diagnosis of Sepsis Predicts Mortality. Shock. 2014;42(5):383-391.
38. Zidar DA, Al-Kindi SG, Liu Y, et al. Association of Lymphopenia With Risk of Mortality Among Adults in the US General Population. JAMA Netw Open. 2019;2(12):e1916526.
39. Hu J, Cai Z, Zhou Y. The Association of Neutrophil–Lymphocyte Ratio with Venous Thromboembolism: A Systematic Review and Meta-Analysis. Clin Appl Thromb Hemost. 2022;28:10760296221130061.

Legends to Figures

Figure 1 **Microvascular recruitment of immune cells during systemic infection**

A, Identities and kinetics of arrested immune cells (1-6h) (**A)** in mice infected with *E. coli* (3-6h) in the. **B**, Unbiased DAVID cluster analysis of significant altered genes (adjusted p <0.05) in uninfected (0h) and infected (3h and 18h) mice.

Boxes indicate different mice. Dots refer to different visual fields (**A**) analyzed from 3 - 9 animals per group. In violin plots, box plots indicate 25th and 75th percentiles and median is marked by bold lines (**A**). P-values were calculated by One-way ANOVA (**A**). *P <0.05, **P <0.01, ***P <0.001, ****P <0.0001.

Figure 2 **$CD4^+$ T cells express and attract major fibrinolysis regulators**

A, Heatmap showing mRNA expression levels of T helper cell genes implicated in negative regulation of coagulations of uninfected (0h) or infected mice (3h, 18h). Boxes indicate different mice. **B**, Associations of TF, uPA, uPAR, PLG and PAI-1 with arrested immune cells in mice infected with *E. coli* (3-6h) in the liver **(**last graph showing percentage of myeloid cells and $CD4^+$ T cells). Dots refer to different visual fields (**B**) analyzed from 3 - 6 animals per group. In violin plots, box plots indicate 25th and 75th percentiles and median is marked by bold lines (**B**). P-values were calculated by One-way ANOVA (**B**). *P <0.05, **P <0.01, ***P <0.001, ****P <0.0001.

Figure 3 **Suppression of intravascular fibrin and microvascular thrombosis by T helper cells**

A-D, Representative images of liver microcirculation (**A,** left) and macrovasculature (**C**) and quantifications of microvascular fibrin deposition and microthrombi in the liver or lung (**A,B,D**) after infection with *E. coli* (**A-C)** or after infection with *S.pneumoniae* (**D**) in T helper cell-depleted mice (αCD4, 1h (**A**), 3h (**B,C),** 6h **(D)**). Values indicate intravascular fibrin-covered area as percentage of total intravascular area in the liver (**A,B,D**) or of intravascular fibrin-covered area per visual field in the lung (**B,D**). Dotted lines indicate vessel walls. Bar, 10 μm (**A**) or 20μm (**C**). Dots refer to different visual fields (**A**) analyzed from 3 animals per group or the mean of at least 5 visual fields per animal (**B,D**). In violin plots, box plots indicate 25th and 75th percentiles and median is marked by bold lines (**A**). P-values were calculated by unpaired two-tailed t-test (**A,B,D**). *P <0.05, **P <0.01, ****P <0.0001.

Figure 4 **Thrombin activatable fibrinolysis inhibitor (TAFI) increases fibrin deposition in absence of CD4$^+$ T cells**

A, Plasmin formation by CD4$^+$ T cells from uninfected and infected (3h) mice. **B-D,** Microvascular fibrin-rich area in liver microcirculation after αCD4 and αUPa treatment (**B**), TAFI neutralization (**C**) or CPI injection (**D**). **E**, Association of TAFI with leukocytes (CD45$^+$) and T helper cells (CD45$^+$ CD3$^+$) 3h after infection. **F,** TAFI colocalization with CD4$^+$ T cell (3h, IgG) or other immune cell rich thrombi (αCD4, 3h). **G,** Association of TAFI with fibrin deposits in vicinity of CD4$^+$ T cells (control) or T cell-free immune cell thrombi (CD4$^+$ T cell depletion)**.** Dots indicate different animals (**B-E,G)** or mean value from 3 independent samples **(A)**. Data shown as means ± s.e.m. P-values calculated by Two-Way ANOVA (**A,C**) or unpaired two-tailed t-test (**B**,**D,E,G**). P values calculated compared to control group (**A**). *P <0.05, **P <0.01, ***P <0.001, **** P<0.0001.

Figure 5 **Fibrin critically drives arrest of T helper cells**

A,**B**, CD4$^+$ T cells or CD4$^+$ RORγt$^+$ cells (**B**) arrested in liver microvessels in *f12*$^{-/-}$ mice (6h) (**A**) or *plg*$^{-/-}$ mice (3h) (**B**) infected with *E. coli*. **C**, Percentage of activated T helper cells (defined as CD38$^+$ or CD69$^+$) in fibrin-negative (-) or fibrin-positive (+) areas (3h). **D,E,** T helper cell activation in the liver microcirculation of rivaroxaban-treated WT mice (**D**) and *f12*$^{-/-}$ mice (3h) (**E**). **F**, Percentage of IFNγ$^+$ T helper cells in rivaroxaban treated mice. **G,** Percentage of T helper cell activation in mice treated with αMHC-II or αIL12p40-antibody prior to infection with *E. coli* (3h). In violin plots, box plots indicate 25th and 75th percentiles and median is marked by bold lines (**A**,**B**). A minimum of 3 biological replicates was analyzed (**A-G)** and dots indicate different animals (**C-G)**. Scale bar, 10μm (**C**). Data shown as means ± s.e.m. P-values calculated by unpaired two-tailed t- test (**A- G**). *P <0.05, **P <0.01, **P <0.01.

Figure 6 **Fibrin activates T helper cells via LFA-1**

A,B Time lapse showing intravascular unidirectional (**A**) and back-forward (**B**) crawling of CMTPX-labeled CD4$^+$ T cells (magenta) by multi-photon intravital imaging (1-6h, *E. coli*). Dragon tails visualize the last 100s of cell movements. Bar, 10 μm **C**, Effect of αLFA-1 antibody on unidirectional migration and arrest of T helper cells in the liver microcirculation analyzed by multi-photon intravital imaging (1-6h). **D**, Percentages of activated CD4$^+$ T cells

arrested in microvessels after treatment with αLFA-1 antibody (3h). **E,** Effect of αLFA-1 antibody on activation of isolated human $CD4^+$ T cells in vitro on poly-L-ornithine- or fibrin-coated surfaces. **L**, Migration of isolated human $CD4^+$ T cells on fibrin- vs. poly-L-orinithine coated surfaces. Lines indicate covered distance by single cells. Speed of cell movements is color coded. Dots indicate different animals (**D**), different videos (**C**) analyzed in at least 3 animals per group, or isolated cells from different donors (**E**). Scale bar 10μm (**A,B**) or 20 μm (**F**). Data shown as means ± s.e.m. P-values calculated by Mann-Whitney test (**C**), unpaired two-tailed t-test (**D)** or Two-Way ANOVA (**E**). *P <0.05, **P <0.01.

Figure 7 **Thrombosis development in human infections is negatively associated with T cell arrest**

A,**B**, $CD4^+$ T cells in pulmonary vessels with diameter <50 μm (**A**) or 50-500 μm (**B**) in patients with SARS-CoV- 2 or influenza virus infections in post-mortem histological analysis of human lung samples with pulmonary infections. **C**, Representative image of thrombus in pulmonary vessels of a patients with severe influenza virus (left) or SARS-CoV-2 infection (right). Bar, 20 μm. **D**, Association of TAFI with leukocyte-free thrombi during SARS-CoV-2 infection. **E**, Correlation between pulmonary thrombosis and intravascular T helper cells Bar, 20μm. Dots indicate different patients (**A,B**,**E**). Values given as mean ± s.e.m. P-values calculated by unpaired two-tailed t-test (**A**,**B**) or Pearson' correlation with 95% confidence interval (**E**). **P <0.01, ***P <0.001.

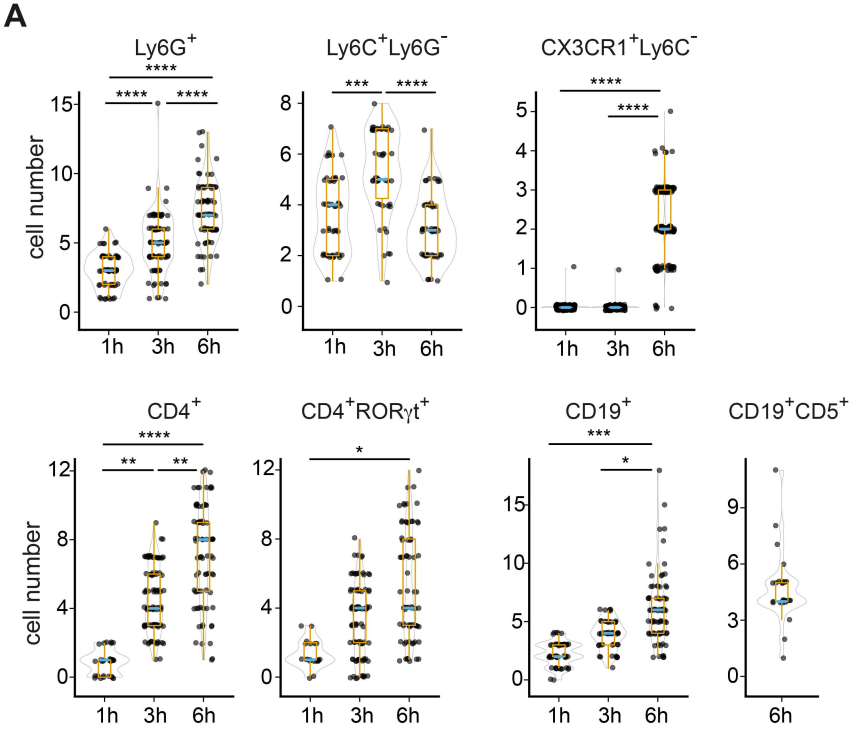
A
Ly6G+
Ly6C+Ly6G-
CX3CR1+Ly6C-
CD4+
CD4+RORγt+
CD19+
CD19+CD5+
cell number
1h
3h
6h

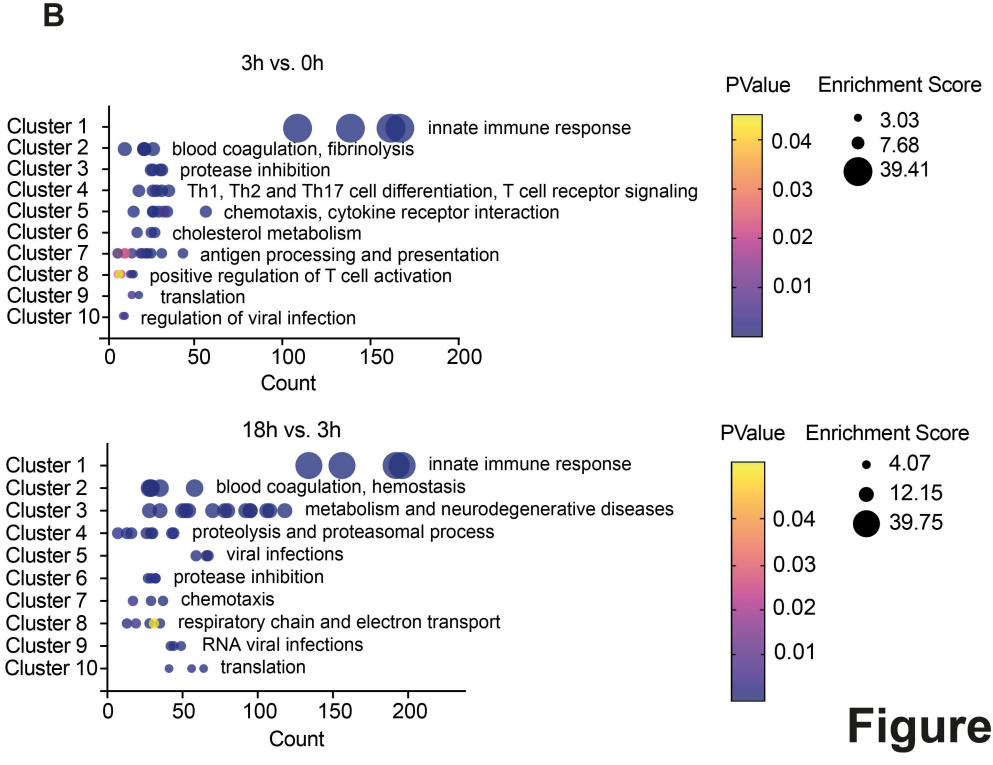
B
3h vs. 0h
Cluster 1 innate immune response
Cluster 2 blood coagulation, fibrinolysis
Cluster 3 protease inhibition
Cluster 4 Th1, Th2 and Th17 cell differentiation, T cell receptor signaling
Cluster 5 chemotaxis, cytokine receptor interaction
Cluster 6 cholesterol metabolism
Cluster 7 antigen processing and presentation
Cluster 8 positive regulation of T cell activation
Cluster 9 translation
Cluster 10 regulation of viral infection
Count
PValue
Enrichment Score
18h vs. 3h
Cluster 1 innate immune response
Cluster 2 blood coagulation, hemostasis
Cluster 3 metabolism and neurodegenerative diseases
Cluster 4 proteolysis and proteasomal process
Cluster 5 viral infections
Cluster 6 protease inhibition
Cluster 7 chemotaxis
Cluster 8 respiratory chain and electron transport
Cluster 9 RNA viral infections
Cluster 10 translation
Count
PValue
Enrichment Score

Figure 1

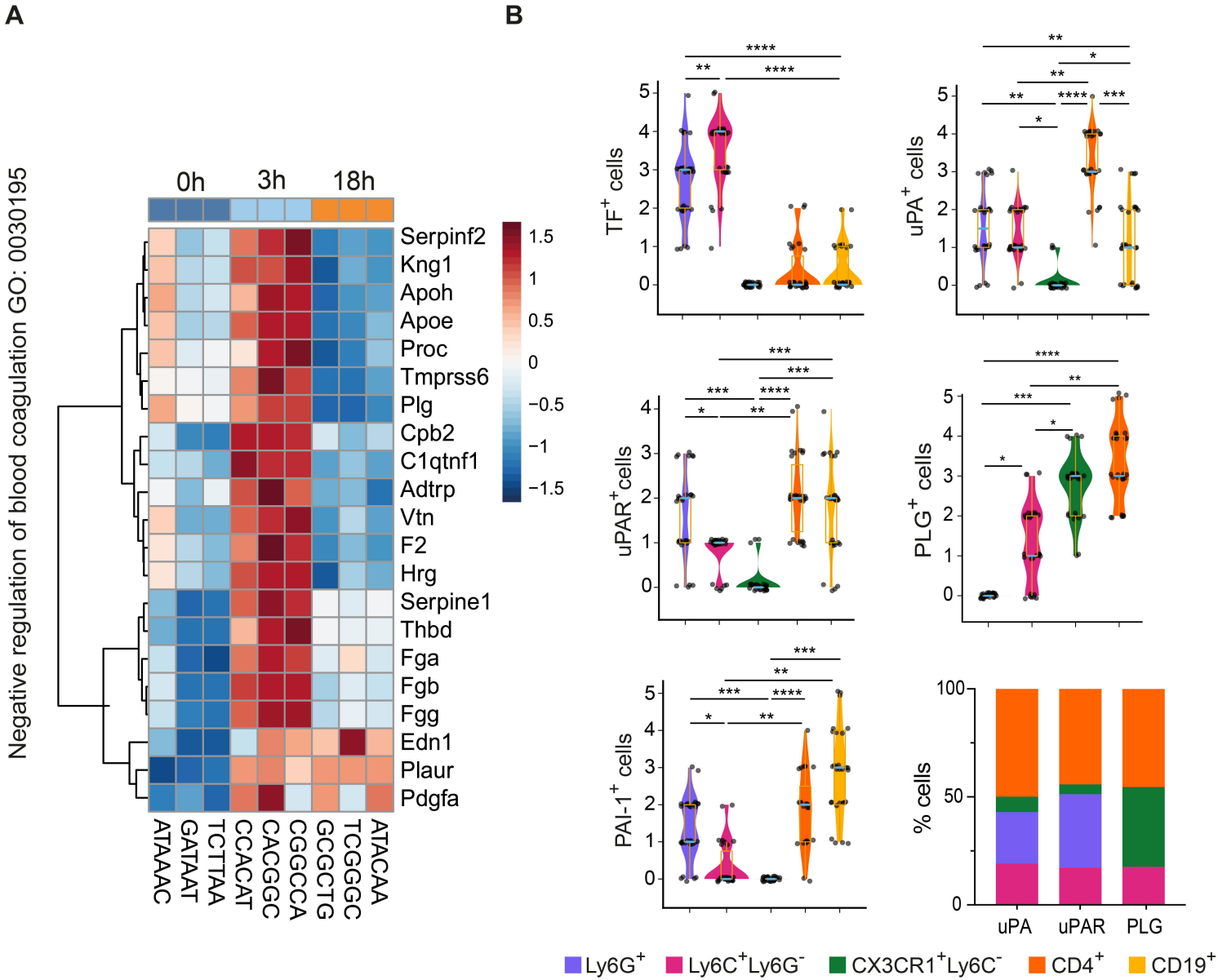
A
Negative regulation of blood coagulation GO: 0030195
0h
3h
18h
Serpinf2
Kng1
Apoh
Apoe
Proc
Tmprss6
Plg
Cpb2
C1qtnf1
Adtrp
Vtn
F2
Hrg
Serpine1
Thbd
Fga
Fgb
Fgg
Edn1
Plaur
Pdgfa
1.5
1
0.5
0
−0.5
−1
−1.5
ATAAAC
GATAAT
TCTTAA
CCACAT
CACGGC
CGGCCA
GCGCTG
TCGGGC
ATACAA
B
TF+ cells
uPA+ cells
uPAR+cells
PLG+ cells
PAI-1+ cells
% cells
100
50
0
uPA
uPAR
PLG
Ly6G+
Ly6C+Ly6G-
CX3CR1+Ly6C-
CD4+
CD19+

Figure 2

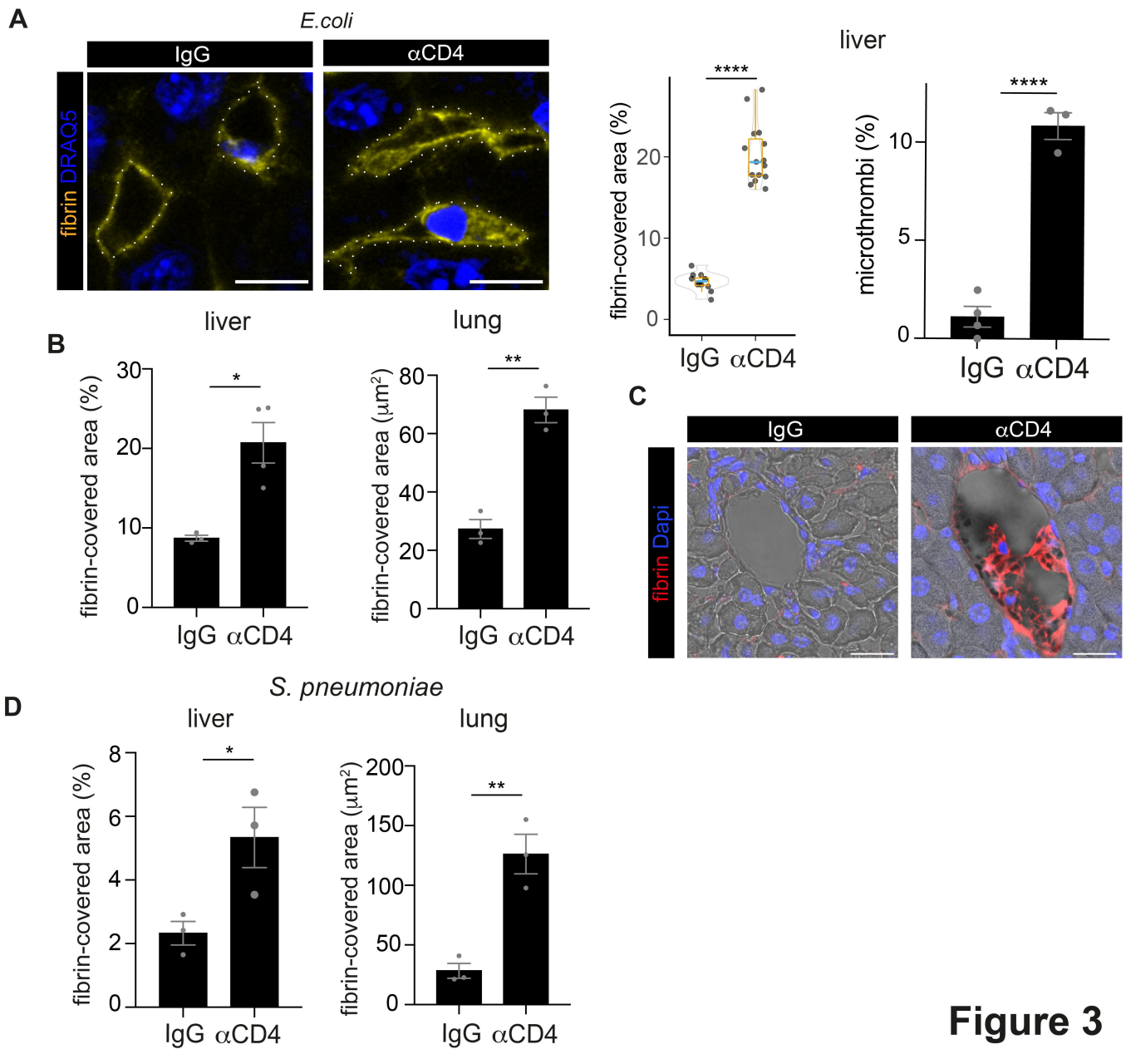
A
E.coli
IgG
αCD4
fibrin DRAQ5
liver
****
fibrin-covered area (%)
IgG αCD4
****
microthrombi (%)
IgG αCD4
B
liver
lung
*
fibrin-covered area (%)
IgG αCD4
**
fibrin-covered area (μm²)
IgG αCD4
C
IgG
αCD4
fibrin Dapi
D
S. pneumoniae
liver
lung
*
fibrin-covered area (%)
IgG αCD4
**
fibrin-covered area (μm²)
IgG αCD4

Figure 3

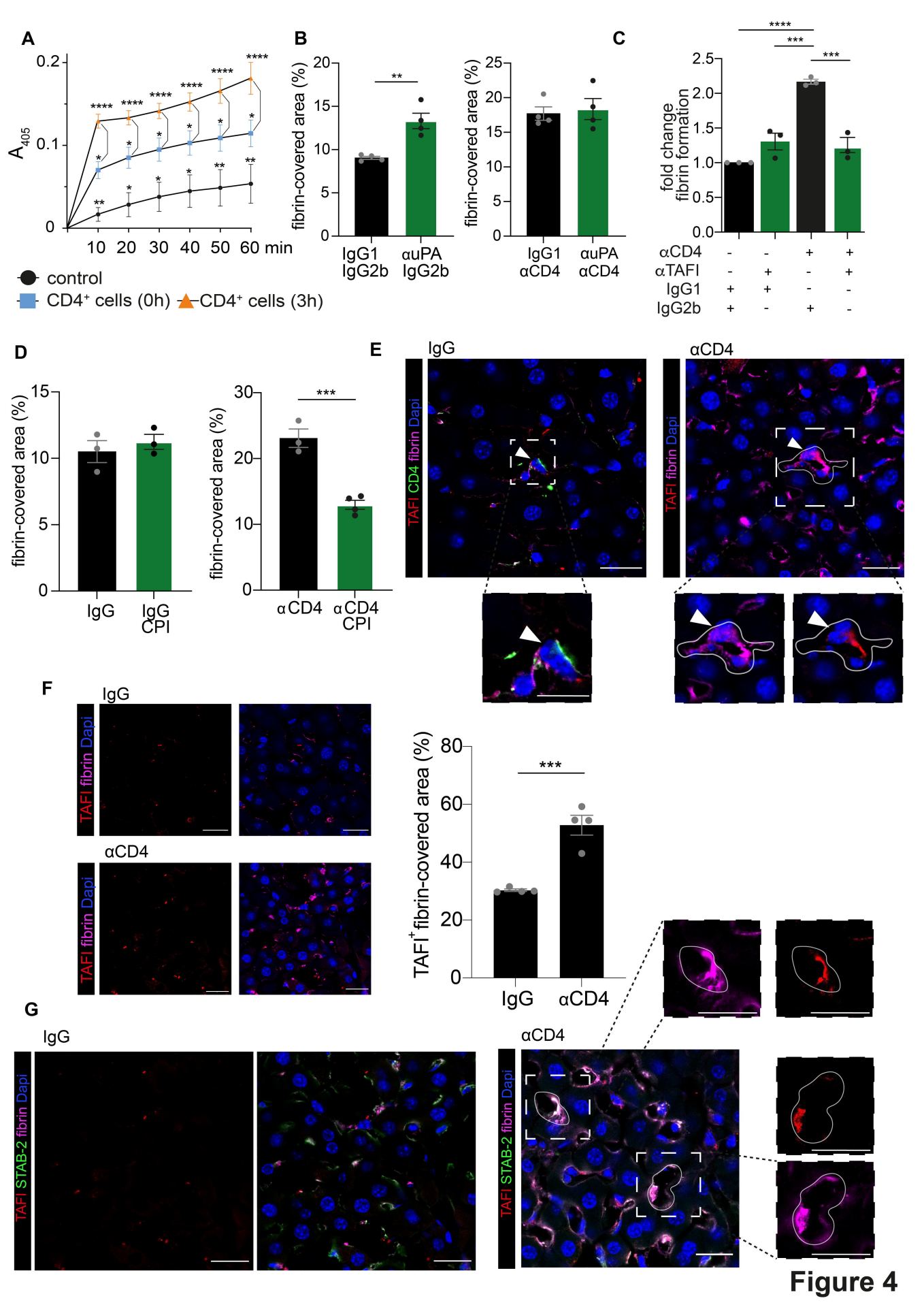
A
B
C
D
E
F
G
A_{405}
control
CD4⁺ cells (0h)
CD4⁺ cells (3h)
10 20 30 40 50 60 min
fibrin-covered area (%)
IgG1 IgG2b
αuPA IgG2b
IgG1 αCD4
αuPA αCD4
fold change fibrin formation
αCD4
αTAFI
IgG1
IgG2b
IgG
αCD4
TAFI CD4 fibrin Dapi
TAFI fibrin Dapi
IgG CPI
αCD4 CPI
TAFI⁺ fibrin-covered area (%)
TAFI STAB-2 fibrin Dapi

Figure 4

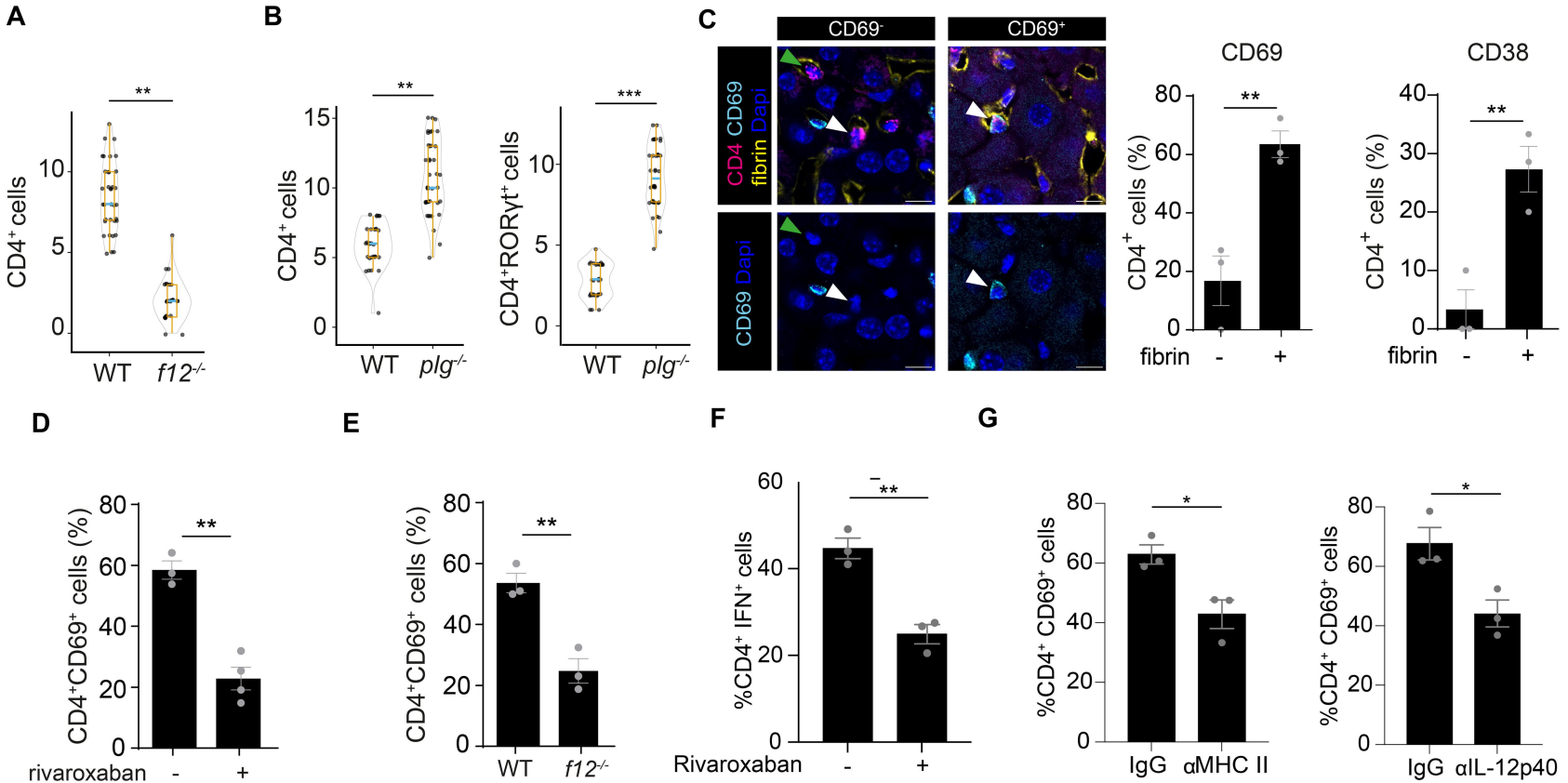
A
B
C
D
E
F
G
CD4⁺ cells
WT
f12-/-
plg-/-
CD4⁺RORγt⁺ cells
CD69⁻
CD69⁺
CD4 CD69 fibrin Dapi
CD69 Dapi
CD69
CD38
CD4⁺ cells (%)
fibrin
CD4⁺CD69⁺ cells (%)
rivaroxaban
%CD4⁺ IFN⁺ cells
Rivaroxaban
%CD4⁺ CD69⁺ cells
IgG
αMHC II
αIL-12p40

Figure 5

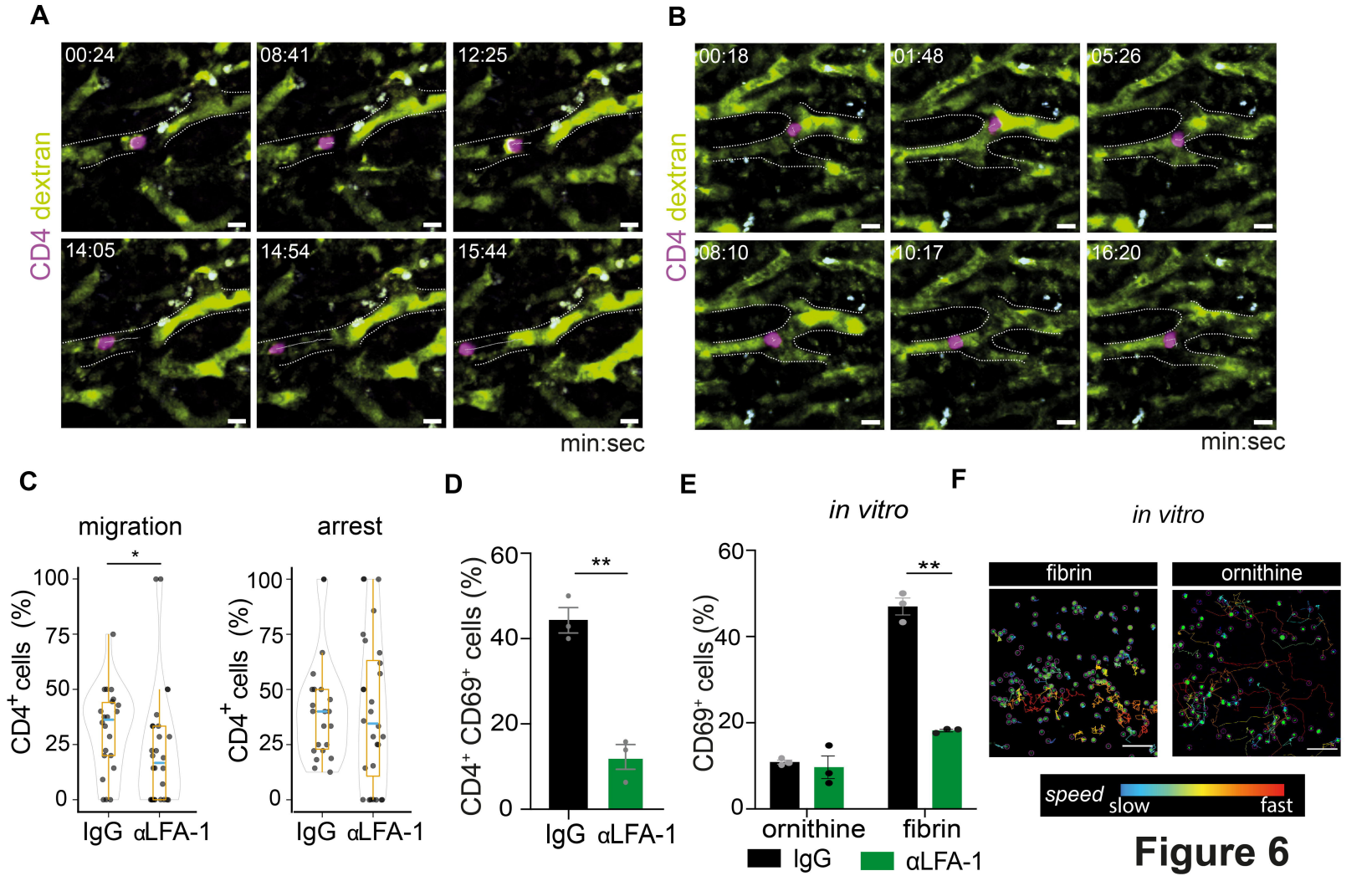
A
00:24
08:41
12:25
14:05
14:54
15:44
CD4 dextran
min:sec
B
00:18
01:48
05:26
08:10
10:17
16:20
CD4 dextran
min:sec
C
migration
arrest
CD4+ cells (%)
IgG
αLFA-1
D
CD4+ CD69+ cells (%)
IgG
αLFA-1
E
in vitro
CD69+ cells (%)
ornithine
fibrin
IgG
αLFA-1
F
in vitro
fibrin
ornithine
speed
slow
fast

Figure 6

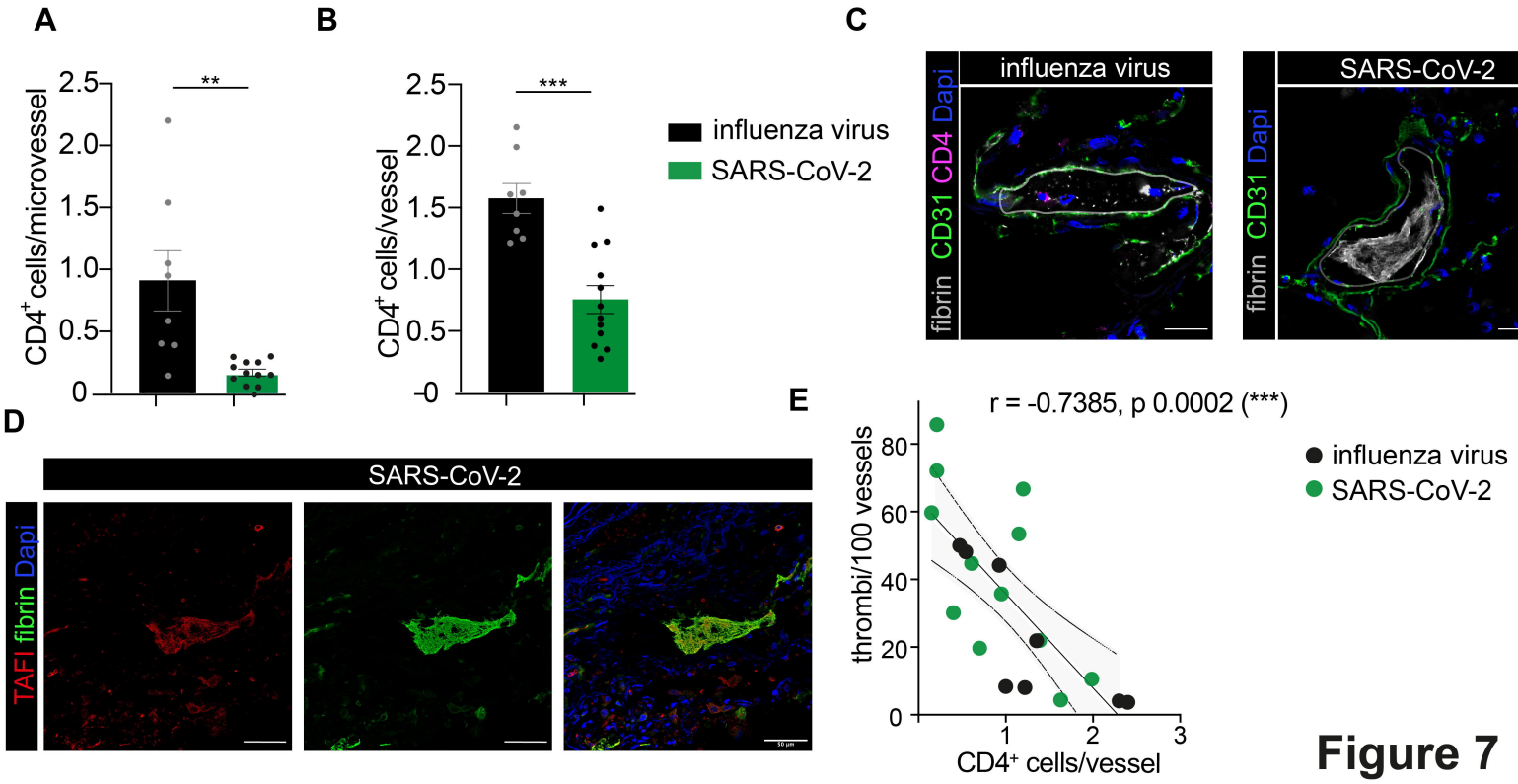
A
B
C
D
E
CD4+ cells/microvessel
CD4+ cells/vessel
**
***
influenza virus
SARS-CoV-2
fibrin CD31 CD4 Dapi
fibrin CD31 Dapi
SARS-CoV-2
TAFI fibrin Dapi
r = -0.7385, p 0.0002 (***)
thrombi/100 vessels
CD4+ cells/vessel

Figure 7

Supplementary Data - **Mutual regulation of CD4$^+$ T cells and intravascular fibrin in infections**

Supplementary Methods

Mouse treatments

The following antibodies were used for depletion of immune cells: CD4$^+$ T cells (αCD4 antibody, GK1.5, 500 µg/mouse, Biolegend)[1,2], neutrophils (αLy6G antibody, 1A8, 400µg/mouse, BioXCell)[3] and classical monocytes (αCCR2 antibody, 20µg/mouse)[4]. The following antibodies or chemicals were used for neutralization prior to infection: αuPA[5] (MU1; 10 mg/kg body weight, provided by Michael Ploug), αTAFI[6] (MA-RT36A3F5, 5 mg/kg body weight, both provided by Paul Declerck), carboxypeptidase inhibitor (CPI, C0279, Sigma)), αLFA-1[7] (M17/4, 100 µg/mouse, BioXCell), αMHC-II[8] (Y-3P, 500 µg/mouse, BioXCell), αIL12p40[9] (C17.8, 500 µg/mouse, BioXCell). Factor VIIa (Novoseven®, Novo Nordisk) was injected via tail vein as previously described[10].

Thrombelastometry and tpa ELISA

Blood was collected from the mice by cardiac puncture using natrium-citrate as a anticoagulant (1:10). Fresh whole blood was immediately used for analysis (<30min) after collection for optimal results. Thus, we combined 300 µl of murine whole citrate blood 20 µl of EXTEM solution (#503-05, Tem Innovations GmbH, Munich, Germany) in reagent cups (#200011, Tem Innovations GmbH) and added 20 µl of StarTEG solution (#503-10, Tem Innovations GmbH). Subsequently, we determined clotting time (CT), clot formation time (CFT), maximum clot firmness (MCF), and the alpha angle at 37 °C.

For the assessment of tpa levels, collected blood was centrifuged at 2500g for 20min at 4°C twice to collect platelet poor plasma. Plasma was added to the ELISA and preparation and measurements were performed according to manufacturer's instructions (biorbyt #orb776434) at 450nm using a plate reader.

Analysis of Kaede mice

Excitation of the photoconvertible protein Kaede with an ultraviolet laser causes the emission to change from green to red Kaede green and Kaede red cells were detected via flow cytometry by their respective fluorescence emission and Th17 cells were identified as CD45$^+$ CD3$^+$ CD4$^+$ IL-

17A$^+$. To exclude γδT cells, kaede green and kaede red cells were analyzed as CD45$^+$ CD3$^+$ CD4$^+$ TCRγδ$^+$ IL-17A$^+$ cells. Less than 15% of CD45$^+$ CD3$^+$ CD4$^+$ IL-17A$^+$ cells represented γδT cells.

CD4 Isolation

The spleen was gently smashed through a 70 µm strainer and cells were collected in MACS buffer (2 mM EDTA, 0.5% bovine serum albumin (BSA) in PBS) and pelleted afterwards (450g, 5min) at room temperature. The pellet was resuspended in cold 1x RBC lysis buffer (8.26 g NH_4Cl, 1.19 g $NaHCO_3$, 0.2 ml 0.5 M EDTA in 1l ddH_2O, pH 7.3) and incubated for 5min. The reaction was stopped by adding MACS buffer (2-3x). Cells were resuspended and passed through a filter (40 µm pore size) and diluted in MACS buffer for cell separation. CD4$^+$ T cells were isolated according to the manufacturer´s instructions (CD4$^+$ T Cell Isolation Kit, 130-104-454, Miltenyi Biotec). Before transfer of T helper cells, lymphocytes were activated in vitro using Dynabeads® CD3/CD28 according to the instructions of the manufacturer (11452D, ThermoFisher) and in some cases treated with 6-Aminocaproic acid (EACA, 10 mM, A2504, Sigma) for 2 hours. Cells were injected i.v. into mice for intravital imaging (2.5 x 10^6) or after factor VIIa-treated mice (4 x 10^6). For RNAseq experiments, plasmin formation assay and Kaede experiments, CD4$^+$ T cells or CD4$^+$IL-17A$^{Katushka+}$T cells were isolated from the liver or lung of uninfected and infected C57BL/6J mice or *kaede* x *Il17a*^{Katushka} mice by flow cytometry. Small tissue pieces of max. 5 mm size were digested for 45min at 37°C with collagenase buffer (10% heat-inactivated FBS, 1% 100× HGPG, 1 mM $CaCl_2$, 1 mM $MgCl_2$, 100 U/ml collagenase IV (Sigma), 10 U/ml DNase I (Roche) in RPMI 1640 (Gibco)), forced through a cell strainer and pelleted by centrifugation (350g, 10min, 4°C). Lymphocytes were separated using 67-40% Percoll gradient, resuspended in FACS buffer (2.5% FCS, 0.03% sodium azide, in PBS) and incubated with antibodies against CD4 (1:400, GK1.5 or RM4-5, Biolegend), CD3 (1:400, 17A2, Biolegend) and CD45 (1:200, 30-F11, Biolegend) for 20min at 4°C in the dark. Red and green Kaede cells were sorted for their IL-17A positivity.

Isolation of human CD4$^+$ T cells

Mononuclear cells were separated by Ficoll-Paque PLUS (400g, 40min, room temperature, diluted 3:1 with isolation buffer (2 mM EDTA in PBS)). Cells were washed (300g, 10min, room temperature) and centrifuged at 200g, 10min at room temperature to remove platelets. The pellet

was diluted in MACS buffer, followed by cell isolation according to the manufacturer´s instructions ($CD4^+$ T Cell Isolation Kit, 130-096-533, Miltenyi Biotec).

In vitro activation and migration of $CD4^+$ T Cells

Microscopic glass slides (Menzel SuperFrost Plus) were coated with 0.01% poly-L-ornithine (Sigma-Aldrich) for 1h at room temperature or with fibrin for 45min at 37°C. For the coating with fibrin, fibrinogen from human plasma (Sigma-Aldrich) was diluted in sterile 0.9% NaCl- solution (2.5 mg/ml) and mixed 3:1 with Thrombin (4U/ml). α-human CD3 antibody (5 µg/ml, HIT3a, Biolegend) was added to the slides and incubated for 3h at 37°C followed by washing 3x with PBS. Isolated $CD4^+$ T cells were resuspended at 1 x 10^6 cells/ml in RPMI Medium 1640 (Glutamax, 2 mM HEPES, 10% FBS, 100 U/ml penicillin, 100 mg/ml streptomycin). The cells were incubated with α-human CD28 antibody (5 µg/ml, CD28.2, Biolegend) at 37°C and 5% CO_2 in a humidified atmosphere. In some cases cells were treated with either an IgG control or an anti-human LFA-1 antibody (20 µg/ml, BioXCell).

To measure T cell migration, 10^5 T helper cells were added to the pre-treated slides and incubated for 30min to allow their tight interaction with the surface. The cells were then visualized every 5min for 3h in a visual field of 500 µm x 500 µm (37°C, 5% CO_2). To track the cell movements, the videos were analyzed using FIJI (Trackmate Plugin[11]). Both, the covered distance as well as the speed of the cells were analyzed.

Immunohistochemistry of frozen samples

All antibodies were unconjugated unless stated otherwise. Sections were stained with secondary antibody (1:1000, AF488, AF546, AF594, AF647, α-rat IgG, α-rabbit IgG, α-mouse IgG, α-goat IgG, Thermo Fisher) for 1h at 4°C. Dapi (1 µg/ml, Sigma Aldrich) or DRAQ5 (5 µM, Biolegend) were used for detection of nuclei.

The following antibodies were used to detect endothelial cells and to analyze formation of fibrin and thrombi: α-stabilin-2 (1:200, MBL), αCD31 antibody (1:50, abcam), α-fibrin IIβ chain antibody (1:200, T2G1, WAK-Chemie Medical GmbH). For analysis of intravascular fibrin deposition, the total vascular area of microvessels (≤ 20 µm diameter) and the fibrin-covered area inside the vessels were measured. Fibrin deposition was either calculated as percentage of fibrin-covered area of total intravascular area or as total amount of intravascular fibrin-covered area per

visual field. All fibrin parameters were calculated from 3 to 5 visual fields (142.7 µm x 142.7 µm) amounting to a total number of >100 analyzed vessels per mouse.

The different types of immune cells were identified by staining with antibodies against Ly6C (1:400, ER-MP20, abcam), Ly6G (1:100, 1A8, Biolegend, primary labelled AF488) or CX3CR1 (1:200, abcam). The different types of T helper cells were detected by staining with the following antibodies: αCD3 (1:100, Novus biologicals), αCD4 (1:150, Biorbyt or 1:150, bioss, AF488), αRORγt (1:100, Biorbyt), αTbet (1:100, antibodies-online), αGATA3 (1:200, 1A12-1D9, Invitrogen), αFoxp3 (1:300, Novusbio). 90.4% of $CD4^+$ cells were identified as $CD3^+$T cells. B cells were stained by using αCD19 (1:100, SouthernBiotech, FITC conjugated) and αCD5 (1:200, eBioscience Invitrogen) antibodies. Lymphocyte activation was analyzed by staining with αCD69 (1:400, R&D Systems) or αCD38 antibodies (1:100, 38C03, Invitrogen).

TF and IL-2 expressions were detected with αTF (1:250, 1H1, Genentech (Roche)) and αIL-2 antibodies (1:400, abcam), respectively. For detection of fibrinolytic mediators, αuPA (1:100, Proteintech or 901420, R&D systems), αuPAR (1:100, abcam), αplasminogen (1:100, abcam), αTAFI (1:100, LSBio) and αPAI-1 (1:100, abcam) antibodies were used. For all immunohistochemical quantifications at least 10 visual fields (142.7 µm x 142.7 µm) were analyzed for each sample. For the verification of the cellular internalization of immune complexes Z-stacks with a stepsize of 1 µm were analyzed. All immunohistochemical images were independently evaluated by two researchers.

Immunohistochemistry of human samples

Samples were fixed with 4% PFA and embedded in paraffin. Three micrometer sections were deparaffinized with ROTI-Histol (Carl Roth) for 20min and re-hydrated through graded ethanol washes. Antigen retrieval was performed with Tris-EDTA buffer (10 mM Tris base, 1 mM EDTA, 0.05% Tween 20, pH 9) for 7min at full pressure in a pressure cooker. After washing with tab water, sections were blocked with 2% BSA, 10% goat serum, 0.1% Tween-20 in TBS for 1h at room temperature and washed afterwards (3 x 3min) with TBS-T. Samples were incubated with primary antibodies (αCD4 (1:200, Bioss); αCD31 (1:100, JC/70A, abcam); αfibrin β chain (1:100, REF 350, LOXO)) for 1h at room temperature or overnight at 4°C, washed and incubated with secondary antibody for 1h at 4°C. Tissue sections were mounted with Fluoroshield Mounting Medium with Dapi (abcam).

For analysis of thrombus formation or vessel occlusion the fibrin-covered area per vessel was measured. Thrombi were defined as aggregates formed by fibrin without or with attached blood cells that obstructed blood vessels by ≥60%. Vessel occlusions were defined as vessel obstructions ≥90%. For each sample at least 50 visual fields (290 µm x 290 µm) were analyzed. All investigations were approved by the local ethics committees (Medical Faculty of Justus-Liebig University: 29/01, Charité Berlin and Medical University of Graz: 32-362ex19/20).

Confocal Microscopy

For imaging of IHC sections and in vitro ICC experiments confocal microscopy was performed as described previously [12] or with an inverted Leica SP8X WLL microscope, equipped with 405 nm laser, WLL2 laser (470 - 670 nm) and acusto-optical beam splitter at the Core Facility Bioimaging of the Biomedical Center of LMU Munich.

Multi-photon intravital imaging

$CD4^+$ T cells isolated from C57BL/6J mice were stained with 10 µM CMTPX (Invitrogen) cell tracker for 20min at 37°C in a humidified atmosphere. CMTPX-labeled $CD4^+$ T cells (2.5 x 10^6, in 200 µl sterile PBS) were i.v. injected into mice 10min after infection with *E. coli*. Mice were anaesthetized by intraperitoneal injection of midazolame (5 mg/kg body weight, Ratiopharm), medetomidine (0.5 mg/kg body weight, Pfizer), and fentanyl (0.05 mg/kg body weight, CuraMed Pharma GmbH). One liver lobe was exposed by a suction ring. FITC-Dextran (2,000 kDa, Sigma Aldrich) was injected via catheter to label the blood flow. For intravital imaging a Multiphoton TrimScope II system (LaVision BioTec) connected to an upright Olympus microscope equipped with a Ti: Sa laser Chameleon Ultra II (coherent tunable in the range 690 to 1,080 nm) was used at 800nm excitation wavelength. The emission was detected by four high sensitive GaAsP (Gallium arsenide phosphide) detectors for single beam scanning and an additional PMT detector for Dodt contrast. Single images were acquired at a depth of 20 to 30 µm with a Z-interval of 2µm. ImSpector Pro (LaVision Biotec) was used as the acquisition software. For each animal, videos were taken over 5-6h. Videos were analyzed using Imaris 9.6.0 (Bitplane, Zurich). Migrating of $CD4^+$ T cells was defined as a movement with a speed between 0.1 µm/s and 1.0 µm/s and an average velocity below 0.35 µm/s. Tracking was performed from the beginning to the end of the locomotion sequence within a video.

Flow Cytometry

Blood was drawn by cardiac puncture and red blood cell lysis was performed. Cells were washed and stained using antibodies against CD45 (biolegend, 30-F11, PerCPCy5.5), CD3 (biolegend, 17A2, APC), CD4 (biolegend, RM4-5, PE), Ly6G (biolegend, 1A8, BV711). Dead cells were stained using Fixable Viability Kit (Zombie, NIR, biolegend) according to manufacturer's instruction. Samples were acquired using an LSR Fortessa Flow Cytometer (BD Biosciences) and analyzed using FlowJo (BD Biosciences).

RNA Sequencing

In contrast to [13], the P5 and P7 sites were exchanged to allow sequencing of the cDNA in read1 and barcodes and UMIs in read2 to achieve better cluster recognition. The library was sequenced on a NextSeq 500 (Illumina) with 67 cycles for the cDNA in read1 and 16 cycles for the barcodes and UMIs in read2. Data were processed using the published Drop-seq pipeline (v1.12) to generate sample- and gene-wise UMI tables [14]. For mapping raw sequencing data reference genome (GRCm38) was used for alignment. Transcript and gene definitions were used according to the GENCODE Version M25. The resulting UMI filtered count matrix was imported into R v3.4.4. Prior differential expression analysis with DESeq2 v1.18.1 (10.1186/s13059-014-0550-8), dispersion of the data was estimated with a parametric fit using the time point as explanatory variable. The Wald test was used for determining differentially regulated genes between different time points. Shrunken log2 fold changes were calculated afterwards. A gene was determined to be differentially regulated if the absolute apeglm shrunken log2 fold change was at least 1 and the adjusted p-value was <0.01. Rlog transformation of the data was performed for visualization and further downstream analysis.

To further investigate the function of T helper cells as coagulation regulators in the context of systemic infection, an unbiased cluster analysis was performed with all significantly altered (adjusted p-value <0.05) genes. This was performed using the bioinformatics database DAVID Huang et al., 2009) by comparing the significantly altered genes with the following defined categories: KEGG Pathway, Gene Ontology Term Biological Process, and the functional categories Biological Process, Cellular Components, and Molecular Function. Subsequently, clusters were created automatically with medium stringency.

Statistical information

All statistical analyses were performed using GraphPad Prism 9 (GraphPad Software). The mean values are given ± s.e.m. The results were compared by unpaired two-tailed t-test, One- or Two-way ANOVA with Tukey's, Sidak's or Dunnett's *post hoc* tests. To test the groups of data for normality the D'Agostino-Pearson omnibus normality test was used. In case of non-normal distributions of data, a Mann-Whitney test was performed instead of unpaired two-tailed t-test. Correlation was determined by Pearson's correlation coefficient in case of normality. Unless otherwise described, all n-values given refer to separate experiments (biological replicates) performed on different animals or independent cell preparations. P values < 0.05 were considered significant.

Data availability

The data that support the findings of this study are available from the corresponding author upon request.

1. Moynihan KD, Opel CF, Szeto GL, et al. Eradication of large established tumors in mice by combination immunotherapy that engages innate and adaptive immune responses. Nat Med 2016;22(12):1402–1410.

2. Klarquist J, Cross EW, Thompson SB, et al. B cells promote CD8 T cell primary and memory responses to subunit vaccines. Cell Rep 2021;36(8):109591.

3. Boivin G, Faget J, Ancey P-B, et al. Durable and controlled depletion of neutrophils in mice. Nat Commun 2020;11(1):2762.

4. Mack M, Cihak J, Simonis C, et al. Expression and Characterization of the Chemokine Receptors CCR2 and CCR5 in Mice. J Immunol 2001;166(7):4697–4704.

5. Lund IK, Jögi A, Rønø B, et al. Antibody-mediated Targeting of the Urokinase-type Plasminogen Activator Proteolytic Function Neutralizes Fibrinolysis in Vivo. J. Biol. Chem. 2008;283(47):32506–32515.

6. Hillmayer K, Vancraenenbroeck R, De Maeyer M, Compernolle G, Declerck PJ, Gils A. Discovery of novel mechanisms and molecular targets for the inhibition of activated thrombin activatable fibrinolysis inhibitor. J. Thromb. Haemost. 2008;6(11):1892–1899.

7. Wang Y, Li D, Nurieva R, et al. LFA-1 Affinity Regulation Is Necessary for the Activation and Proliferation of Naive T Cells. J. Biol. Chem. 2009;284(19):12645–12653.

8. Stefanová I, Dorfman JR, Germain RN. Self-recognition promotes the foreign antigen sensitivity of naive T lymphocytes. Nature 2002;420(6914):429–434.

9. Chiba S, Baghdadi M, Akiba H, et al. Tumor-infiltrating DCs suppress nucleic acid–mediated innate immune responses through interactions between the receptor TIM-3 and the alarmin HMGB1. Nat Immunol 2012;13(9):832–842.

10. Massberg S, Grahl L, von Bruehl M-L, et al. Reciprocal coupling of coagulation and innate immunity via neutrophil serine proteases. Nat Med 2010;16(8):887–896.

11. Tinevez JY, Perry N, Schindelin J, et al. TrackMate: An open and extensible platform for single-particle tracking. Methods 2017;11580–90.

12. von Brühl ML, Stark K, Steinhart A, et al. Monocytes, neutrophils, and platelets cooperate to initiate and propagate venous thrombosis in mice in vivo. J. Exp. Med. 2012;209(4):819–835.

13. Parekh S, Ziegenhain C, Vieth B, Enard W, Hellmann I. The impact of amplification on differential expression analyses by RNA-seq. Sci. Rep.;6.

14. Macosko EZ, Basu A, Satija R, et al. Highly parallel genome-wide expression profiling of individual cells using nanoliter droplets. Cell 2015;161(5):1202–1214.

15. Huang DW, Sherman BT, Lempicki RA. Bioinformatics enrichment tools: paths toward the comprehensive functional analysis of large gene lists. Nucleic Acids Res 2009;37(1):1.

16. Huang DW, Sherman BT, Lempicki RA. Systematic and integrative analysis of large gene lists using DAVID bioinformatics resources. Nat. Protoc. 2009 4:1 2008;4(1):44–57.

Supplementary Fig. 1 **T helper cell subtypes and fibrin homeostasis in systemic infection**

A,**D**, T helper cell subsets in the liver microcirculation (**A**) and association of uPA with different subsets (**D**) (*E. coli*, 1h). **B**, Kinetics of intravascular fibrin deposition after *E. coli* infection. **C**, Clotting time, clot formation time, medium clot firmness and alpha angle measured by thrombelastometry in murine whole blood in uninfected (0h) and infected (3h) mice. **D,** tpa levels in murine plasma in uninfected (0h) and infected (3h) mice. **E**, Percentage of $CD4^+$ T cells of $CD45^+$ leukocytes in the blood of mice treated with αCD4 or control antibody (3h after infection). **F**, AST and ALT serum levels in the blood of uninfected mice as well as in infected mice treated with αCD4 or control antibody (3h). Dots represent different animals (**A**,**C-E**,**G**) or different visual fields in at least 3-9 animals per group (**B**). Data given as means ± s.e.m (**A**,**C-E**,**G**). P-value calculated by One-way ANOVA (**A**,**B**,**E**) or unpaired two-tailed t-test (**D**). *P <0.05, **P <0.01, ***P <0.001, ****P <0.0001.

Supplementary Fig. 2 **Differential effects of innate immune cells vs. $CD4^+$ T cells on fibrin deposition**

A,**B** Microvascular fibrin deposition in the liver after depletion of neutrophils (αLy6G, 3h, **A** left), classical monocytes (αCCR2, 1h, **A**, right) or T_{regs} (αCD25, 3h, **B**). **C**, Plasmin formation by isolated human T helper cells obtained from 3 different human donors. **D,** Fold change in microvascular fibrin deposition in the liver after injection of activated $CD4^+$ T cells, FVIIa and infection with *E. coli* (3h). Red line indicates fibrin deposition in FVIIa treated mice without $CD4^+$ cell injection. Dots represent different animals (**A**,**B**,**D**) or different donors (**C**). Data given as means ± s.e.m (**A**,**C**,**D,F**). P-value calculated by One-way ANOVA (**A-C**,**G**) or unpaired two-tailed t-test (**F,H**). *P <0.05, **P <0.01, ****P <0.0001.

Supplementary Fig. 3 **T cell arrest and activation at the peak of fibrin formation**

A,**B** Microvascular fibrin deposition in *f12*$^{-/-}$ mice (**A**) and after rivaroxaban treatment of WT mice (3h, *E. coli*) (**B**). **C**, Arrested $CD4^+$ T cells and RORγt$^+$ cells in the liver microcirculation after treatment with rivaroxaban. **D**, Heatmap showing mRNA expression levels of T helper cell

genes implicated in T cell activation (GO: 0042110) of uninfected (0h) or infected mice (3h, 18h). **E,** CD69 expression of T helper cells in a thrombus in the macrovasculature (3h). **F,** Percentage of T helper cells that are positive for fibrin, CD69 and IFNγ. Dots indicate different animals (**A-C,F**). Data shown as means ± s.e.m. P- values calculated by unpaired two-tailed t-test (**A-C,F)**.*P <0.05, **P <0.01, ***P <0.001.

Supplementary Fig. 4 **Origin of liver-associated T helper cells**

A, The small intestine of *kaede x Il7a*^{kat} transgenic mice was exposed to UV light, *E. coli* were injected i.v. and liver and lung were harvested. **B**, Kaede red- and green-emitting cells were sorted via flow cytometry for IL-17A^{+} cells and IL-17A^{-} cells in the liver (left) and lung (right). Dots indicate different animals . Data given as means ± s.e.m. P-value calculated by unpaired two-tailed t-test . *P <0.05.

Supplementary Fig. 5 **Regulation of fibrin homeostasis and LFA-1 dependent activation of CD4^{+} T cells**

A, Effect of rivaroxaban treatment on unidirectional migration of T helper cells 1-6h after infection with *E. coli* analyzed by multi-photon intravital microscopy. **B,** Percentage of IFNγ^{+} T helper cells either fibrin positive or negative in αLFA-1 treated mice. **C,** Effect of αLFA-1 antibody on plasmin formation by resting (Trest) or activated (Tact) human CD4^{+} T cells. Dots indicate different animals (**B**), different donors (**C**) or different videos of 3 animals per group (**A**). A minimum of 3 biological replicates was analyzed. Data shown are means ± s.e.m. P-values were calculated by Two-way ANOVA (**B**) or One-way ANOVA (**C).** *P <0.05, **P <0.01, *** P <0.001, ****P <0.0001.

Supplementary Fig. 6 **Thrombotic vessel occlusions in patients with SARS-CoV-2 and influenza virus infections**

A, Patient characteristics **B**, Number of thrombi and vessel occlusions in lungs of patients infected with influenza virus or SARS-CoV-2. Data are means ± s.e.m.. P-values calculated by unpaired two-tailed t-test (**B**). *P <0.05.

Supplementary Videos

Supplementary Video S1 Intravital imaging of T helper cell movements in the liver microcirculation during infection

Intravital multi-photon microscopy of the liver microcirculation of mice infected with *E. coli* (1h-6h). Representative video of experiments on 3 different mice. Videos show representative unidirectional migration and backward-forward movements of $CD4^+$ T cells. $CD4^+$ T cells (CMPTX, red), blood flow (FITC-dextran, green), Kupffer cells (autofluorescence, white/grey). Bar, 10 μm. Videos related to Extended Fig. 4**A**,**B**.

Supplementary Video S2 Effect of LFA-1 neutralization on intravascular migration of $CD4^+$ T cells

Intravital multi-photon microscopy of the liver microcirculation of *E. coli*-infected mice treated with αLFA-1 antibody or control antibody (1h-6h). Representative video of experiments on 3 different mice per group. $CD4^+$ T cells (CMPTX, red), blood flow (FITC-dextran, green), Kupffer cells (autofluorescence, white/grey). Bar, 50 μm. Videos related to Fig. 4**C**.

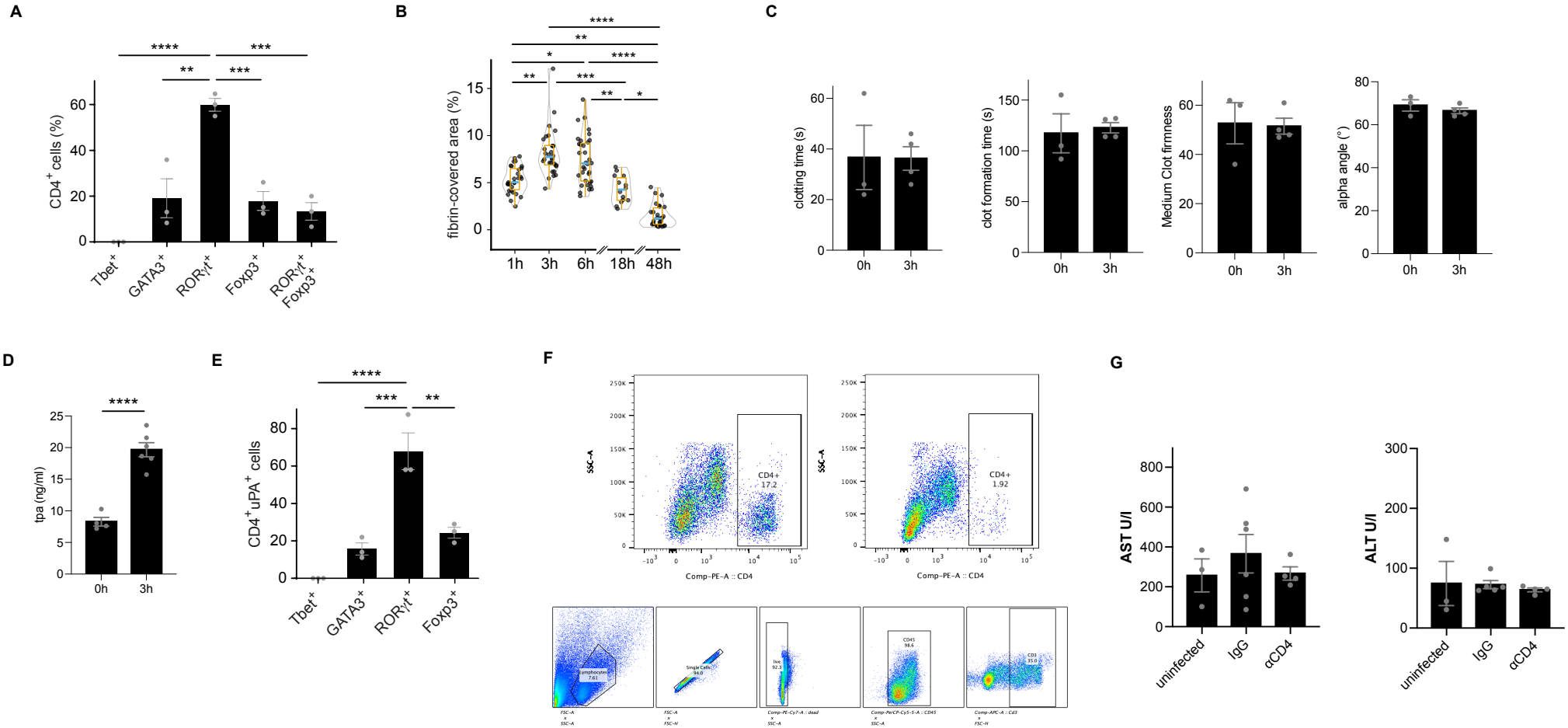

Supplementary Figure 1

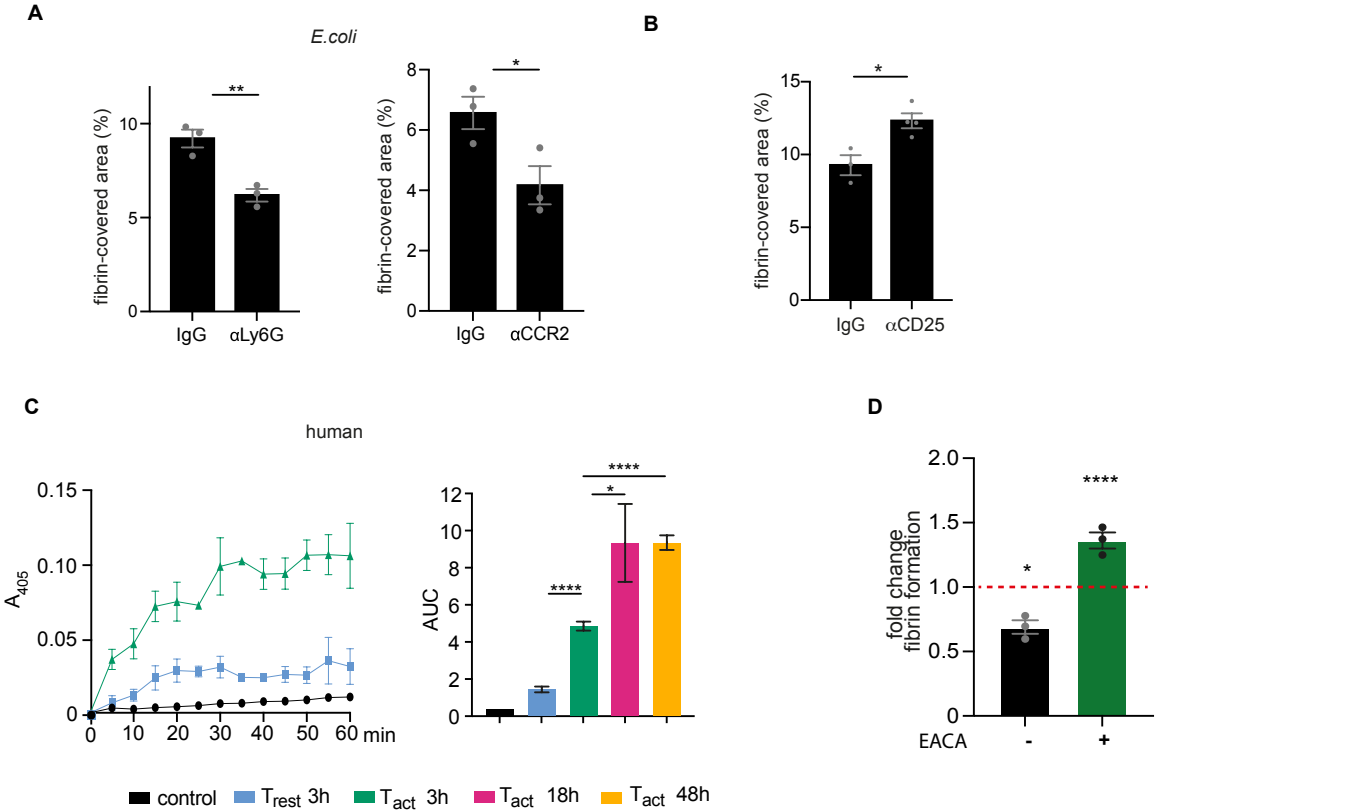

Supplementary Figure 2

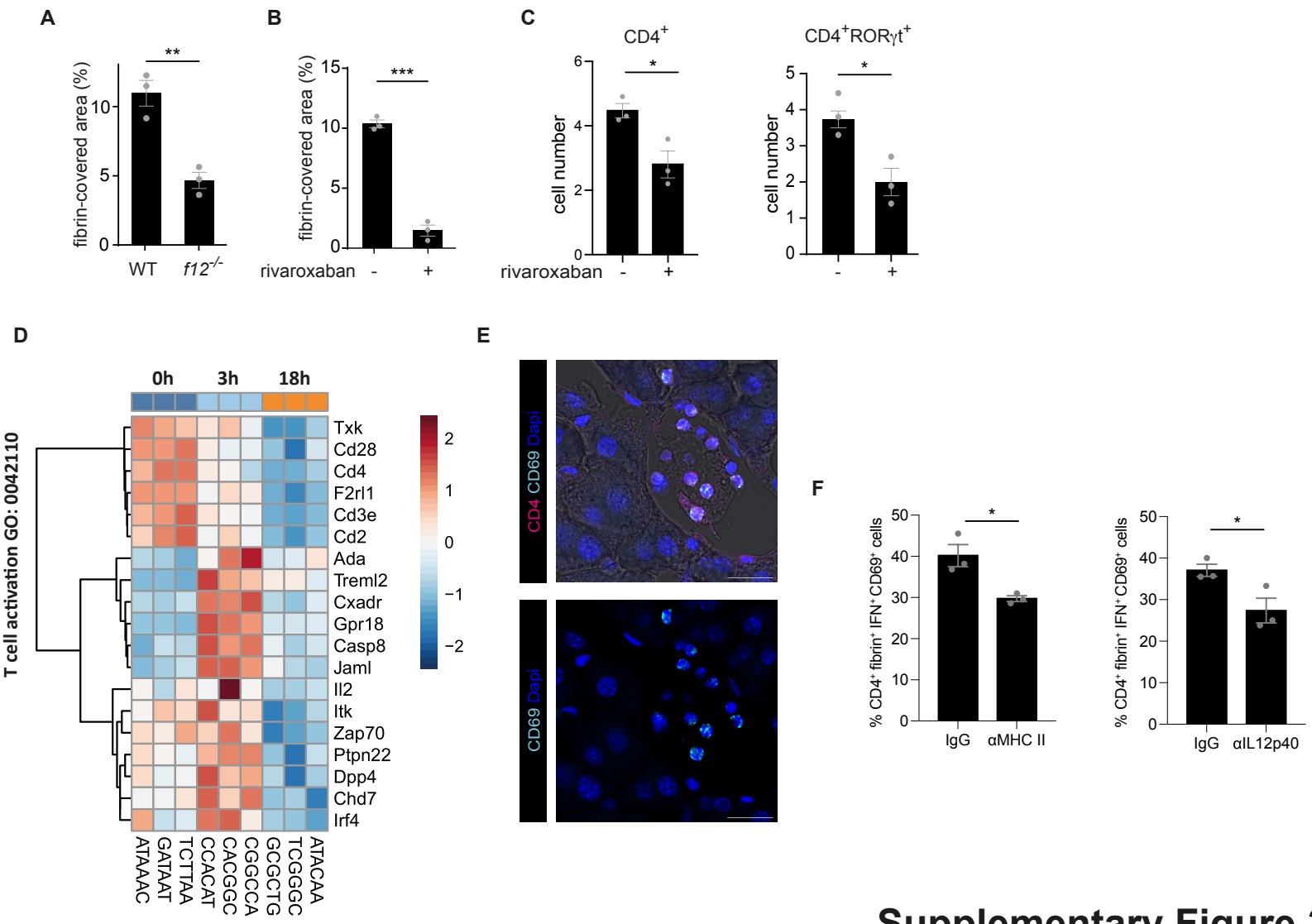

Supplementary Figure 3

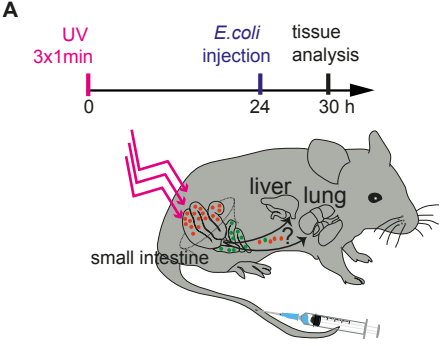

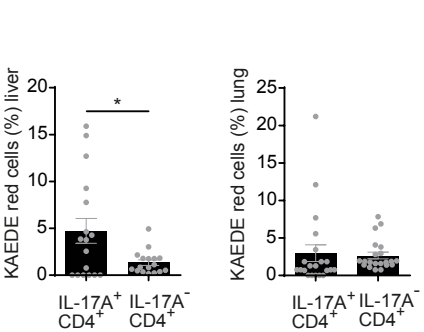

Supplementary Figure 4

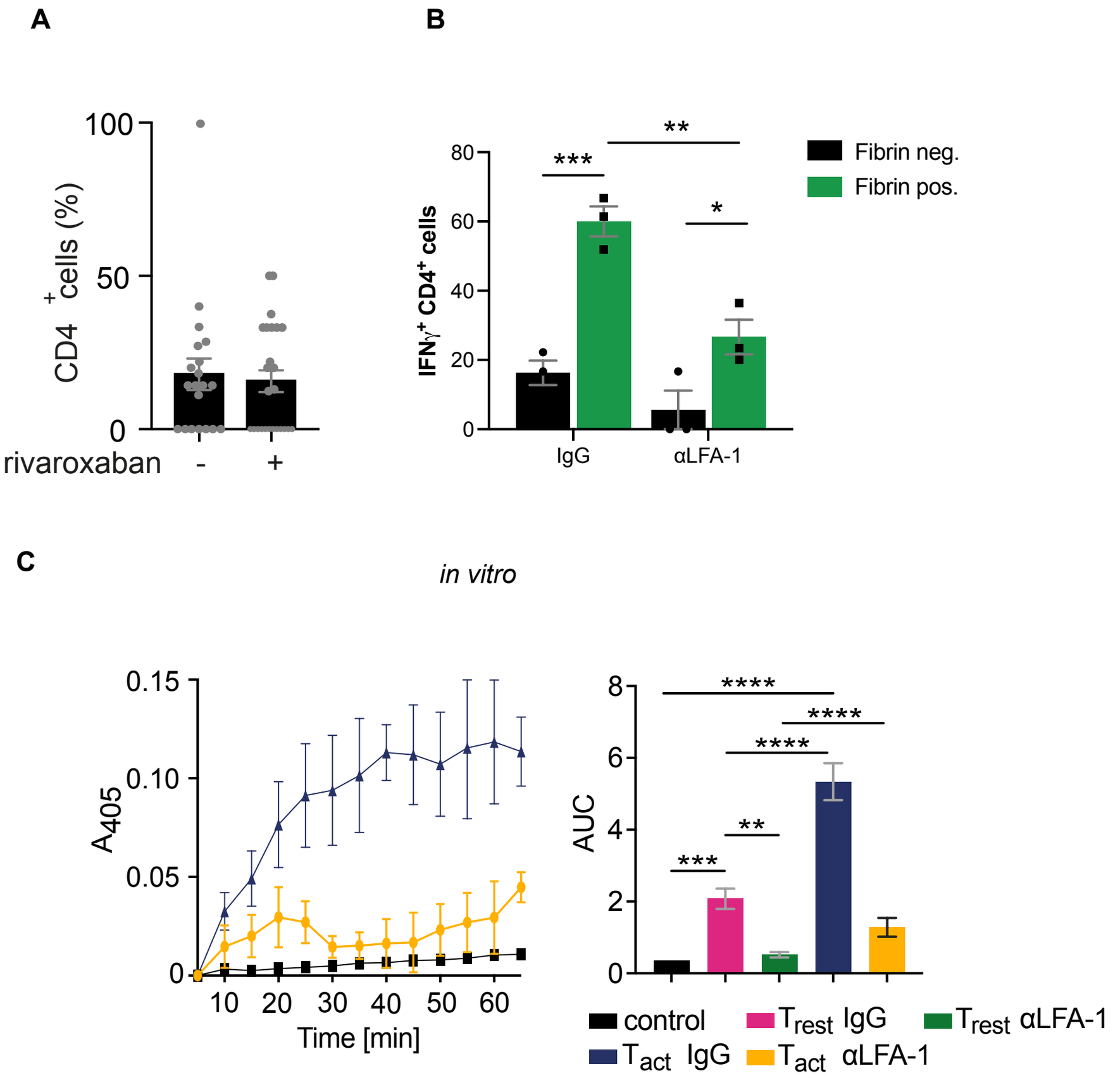

Supplementary Figure 5

A

patient	cohort	sex	age	BMI	active cancer	ECMO	catecholamine requirement
1	Covid-19	female	80	25.5	no	no	yes
2	Covid-19	female	81	*	no	no	no
3	Covid-19	male	83	23	no	no	yes
4	Covid-19	male	79	32	yes	no	no
5	Covid-19	male	85	27.2	no	no	no
6	Covid-19	female	92	24	no	no	yes
7	Covid-19	female	71	27	no	no	yes
8	Covid-19	male	77	35	no	no	yes
9	Covid-19	male	71	23	no	no	yes
10	Covid-19	male	65	42	no	no	no
11	Covid-19	female	93	28	no	no	yes
12	Covid-19	male	67	26	no	no	no
13	Influenza	female	74	33	no	no	yes
14	Influenza	female	81	26	no	no	yes
15	Influenza	female	65	39	no	no	yes
16	Influenza	male	90	21	no	no	yes
17	Influenza	male	61	23	no	no	no
18	Influenza	male	78	24	no	no	yes
19	Influenza	male	43	24.6	no	yes	no
20	Influenza	male	53	*	no	yes	yes

B

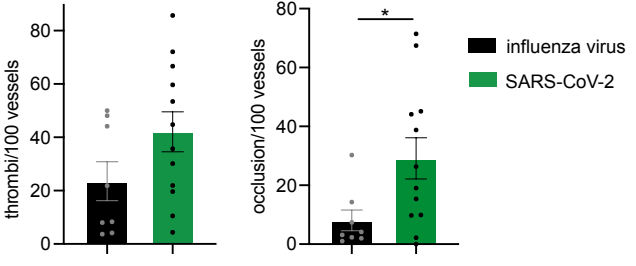

Supplementary Figure 6